The Company of Biologists

STEM CELLS AND REGENERATION

RESEARCH ARTICLE

Signalling codes for the maintenance and lineage commitment of embryonic gastric epithelial progenitors

Sergi Sayols[1], Jakub Klassek[1], Clara Werner[1], Stefanie Möckel[1], Sandra Ritz[1], Maria Mendez-Lago[1] and Natalia Soshnikova[2,*]

ABSTRACT

The identity of embryonic gastric epithelial progenitors is unknown. We used single-cell RNA-sequencing, genetic lineage tracing and organoid assays to assess whether *Axin2*- and *Lgr5*-expressing cells are gastric progenitors in the developing mouse stomach. We show that $Axin2^+$ cells represent a transient population of embryonic epithelial cells in the forestomach. $Lgr5^+$ cells generate both glandular corpus and squamous forestomach organoids *ex vivo*. Only $Lgr5^+$ progenitors give rise to zymogenic cells in culture. Modulating the activity of the WNT, BMP and Notch pathways *in vivo* and *ex vivo*, we found that WNTs are essential for the maintenance of $Lgr5^+$ epithelial cells. Notch prevents differentiation of the embryonic epithelial cells along all secretory lineages and hence ensures their maintenance. Whereas WNTs promote differentiation of the embryonic progenitors along the zymogenic cell lineage, BMPs enhance their differentiation along the parietal lineage. In contrast, WNTs and BMPs are required to suppress differentiation of embryonic gastric epithelium along the pit cell lineage. Thus, coordinated action of the WNT, BMP and Notch pathways controls cell fate determination in the embryonic gastric epithelium.

KEY WORDS: BMP, Gastric stem cell, Notch, Stomach, Single-cell RNA-sequencing, WNT

INTRODUCTION

The stomach has a number of vital functions, including food digestion, secretion of hormones and host defence against microorganisms. These functions depend on the correct specification and maintenance of differentiated cell types within the stomach epithelium. In mice, the stomach epithelium is composed of two types: keratinized squamous epithelium of the forestomach and glandular epithelium of the corpus and antrum (Willet and Mills, 2016). In the corpus, glandular epithelial cells differentiate along four secretory lineages: mucous pit cells (expressing MUC5AC and TFF1), mucous- and/or enzyme-secreting zymogenic cells [characterized by expression of TFF2 and MUC6 in precursors and by GIF, MIST1 and gastricsin (PGC) in mature chief cells], acid-producing parietal cells (expressing ATP4a/b) and endocrine cells expressing various hormones (Willet and Mills, 2016). The antral epithelium consists of pit cells, mucous neck cells that also express markers of chief cells and endocrine cells.

Gastric epithelial cells are constantly challenged by the harsh environment, pathogens and xenobiotics. Renewal of the epithelium is supported by gastric stem cells and progenitor cells. The search for multipotent stem cells within the stomach epithelium has been the focus of extensive research. Previous studies defined cell populations expressing either *Sox2*, *Mist1* (*Bhlha15*), *Cckbr*, *Runx1*, *Lrig1*, *Bmi* or *Stmn1* as stem cells that can both self-renew and generate differentiated cells at steady state (Arnold et al., 2011; Hayakawa et al., 2015a,b; Matsuo et al., 2017; Choi et al., 2018; Schweiger et al., 2018; Yoshioka et al., 2019; Han et al., 2019). Upon injury, $TROY^+$ ($Tnfrsf19^+$) and $Lgr5^+$ post-mitotic chief cells de-differentiate in proliferative stem cells and regenerate the gastric epithelium (Stange et al., 2013; Leushacke et al., 2017). Furthermore, neonatal $Lgr5^+$ cells contribute to the mature antral epithelium during stomach homeostasis (Barker et al., 2010). Because the embryonic gastric epithelial progenitors remain undefined, it is unknown whether these molecularly distinct gastric stem cells come from common or molecularly functionally distinct embryonic progenitors.

Cell lineage specification commences in the mouse stomach at approximatively embryonic day (E)13.5 (Willet and Mills, 2016). Little is known about factors and pathways regulating the commitment of embryonic epithelial cells towards either stem cell/progenitors or secretory lineages. Several signals, including fibroblast growth factor 10 (FGF10), Notch and WNT, enhance proliferation of embryonic gastric epithelial cells (Spencer-Dene et al., 2006; Kim and Shivdasani, 2011; McCracken et al., 2017). In contrast, bone morphogenetic protein (BMP) signalling negatively regulates proliferation of endocrine precursor cells (Maloum et al., 2011). Apart from regulating cell division rates, FGF10 signalling is essential for patterning of the embryonic stomach along the rostral-caudal axis (Spencer-Dene et al., 2006). In the absence of *Fgf10* or its receptor *Fgfr2b*, the glandular epithelium is not correctly specified, which leads to the loss of the parietal cell lineage. Moreover, WNT/β-catenin mediated signalling instructs the glandular epithelial cells to become corpus epithelium (McCracken et al., 2017). Furthermore, BMP signalling supports differentiation of the epithelial progenitors along the parietal cell lineage (Maloum et al., 2011). The ablation of BMP receptor 1a (Bmpr1a) in the gastric epithelium leads to the reduction of parietal cell numbers.

Here, we used single-cell RNA sequencing (scRNA-seq), lineage tracing and organoid cultures to gain insight into the function and regulation of gastric epithelial progenitors during mouse embryogenesis. We found that $Axin2^+$ cells represent a transient population of embryonic epithelial cells in the forestomach. On the other hand, $Lgr5^+$ epithelial cells generate corpus organoids and retain self-renewal and differentiation capacity *ex vivo*. Inhibition of

DEVELOPMENT

signalling pathways *in vivo* and *ex vivo* showed a role for BMP, Notch and WNT signalling during differentiation of the embryonic gastric epithelium.

RESULTS

Cellular composition of the embryonic stomach

To characterize cell lineages within the embryonic stomach at the initiation of epithelial differentiation, we performed scRNA-seq of gastric cells isolated from mouse embryos at E13.5. Single cells expressing pan-epithelial marker EpCAM or EpCAM-negative non-epithelial cells were isolated by fluorescent activated cell sorting (FACS) and processed using SMARTer technology (Fig. 1A,B; Fig. S1A). We used 250 EpCAM$^+$ and 225 EpCAM$^-$ cells that passed quality control thresholds for further analysis. Unsupervised clustering analysis revealed eight cell populations (Fig. 1C). EpCAM$^+$ cells formed three clusters representing forestomach, corpus and antral epithelium (Fig. 1D,E,I). Specifically, cells in the forestomach (Fs) cluster had high expression of *Krt5*, *Krt15*, *Trp63* and *Shh* (Fig. 1E; Fig. S1B). Cells in the corpus cluster (Co) highly

expressed embryonic pepsinogen chymosin (*Cym*) (Fig. 1E,F), *Fkbp11* and *Cxcl15* (Fig. S1B). Furthermore, several transcription factors, such as *Isl1* and *Osr1*, were expressed in the corpus but not in antral cells (Fig. S1B). In contrast, the antral cells (An) showed expression of transcription factors *Pdx1*, *Nkx6-2* and *Nkx6-3* (Fig. S1B; Fig. 1G,E) as well as genes associated with the duodenal epithelium, *Arg1*, *Lgals4* and *Nepn* (Fig. S1B). Only a few cells were positive for parietal lineage marker *Atp4b*, mucous neck/zymogen lineage markers *Pgc* and *Tff2* as well as pit lineage marker *Muc5ac* in both corpus and antral epithelium (Fig. S1C), suggesting that the embryonic gastric epithelial progenitors had already initiated differentiation by E13.5.

The largest mesenchymal cluster consisted of both fibroblasts and myofibroblasts (Fb) expressing various collagens, including *Col1a2*, *Col3a1* and *Col6a1* as well as *Fn1*, *Pdgfra* and *Pdgfrb* (Fig. 1H,J; Fig. S1D). Myofibroblasts also expressed smooth muscle associated genes, such as *Acta2*, *Myh11*, *Cnn1* and *Myom1* (Fig. S1D), suggesting that myofibroblasts initiated differentiation. Mesenchymal cluster 2 expressed mesenchymal genes, including
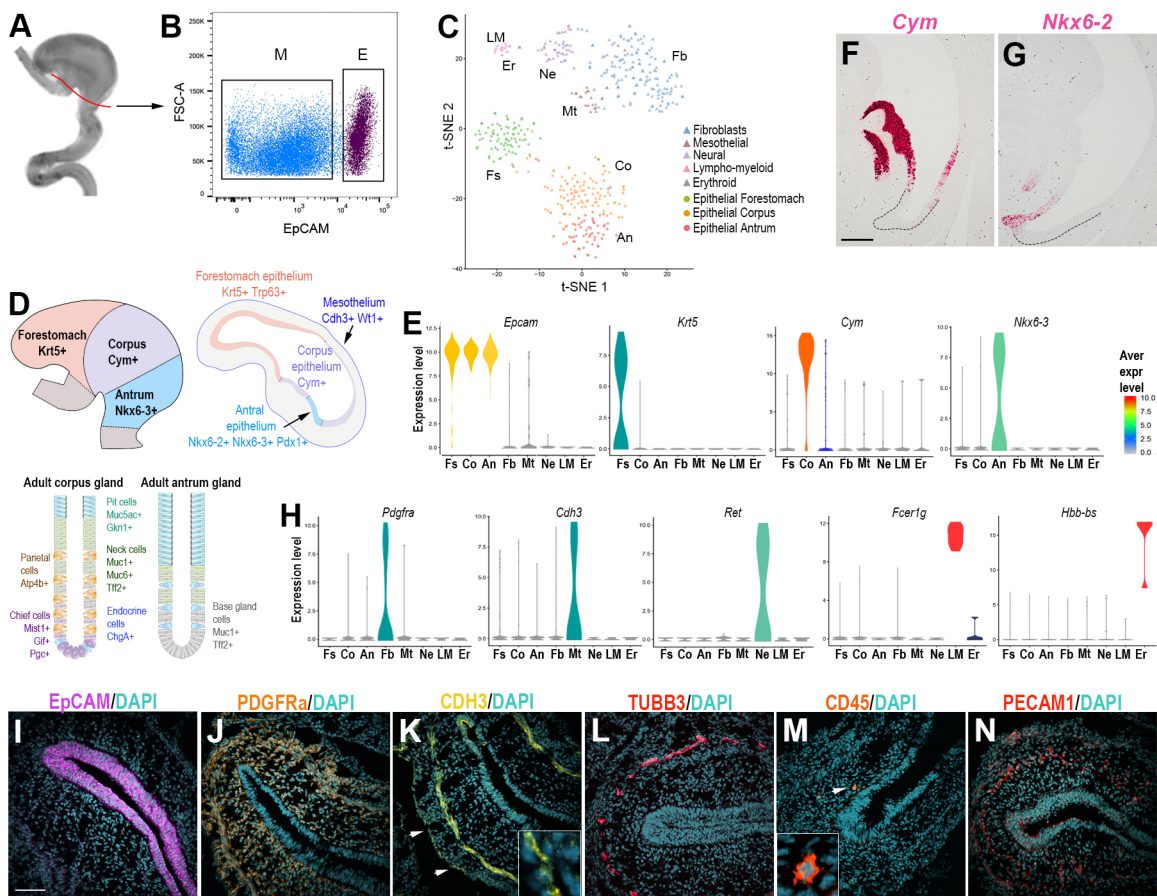

Fig. 1. Single-cell transcriptome analysis of embryonic stomach. (A) Outline of dissection strategy of mouse stomach at E13.5. (B) Representative FACS profile showing EpCAM$^+$ gastric epithelial cells (violet) and EpCAM$^-$ gastric mesenchymal cells (blue) at E13.5 (*n*=39). (C) T-stochastic neighbour embedding (t-SNE) plot of mouse embryonic gastric cells. Single cells are coloured by cluster annotation. (D) Schematic of the mouse stomach showing three domains: forestomach, corpus and antrum (top left). Cross-section of the mouse stomach showing *Krt5$^+$Trp63$^+$* forestomach epithelium, *Cym$^+$* corpus epithelium, *Pdx1$^+$Nkx6-2$^+$Nkx6-3$^+$* antral epithelium and *Cdh3$^+$Wt1$^+$* mesothelium (top right). Cellular composition and markers for each cell type of the adult corpus gland (bottom left) and of the antrum gland (bottom right). (E) Violin plots for pan-epithelial marker EpCAM across clusters as well as for marker genes for forestomach (Fs), corpus (Co) and antrum (An) epithelium. Colour scale reflects normalized expression for each cell cluster. (F,G) Single-molecule RNA ISH for a marker of the corpus epithelium *Cym* (F) and a marker of the antral epithelium *Nkx6-2* (G) on mouse stomach at E13.5. (H) Violin plots for marker genes for fibroblast (Fb), mesothelial (Ms), enteric neural (Ne), lympho-myeloid (LM) and erythroid (Er) cell lineages. Colour scale reflects normalized expression for each cell cluster. (I-N) Immunostaining of E13.5 mouse stomach showing distribution of EpCAM$^+$ epithelial (I), PDGFRa$^+$ fibroblast (J), P-cadherin/CDH3$^+$ mesothelial (K), TUBB3$^+$ enteric neural (L), CD45/PTPRC$^+$ lympho-myeloid (M) and CD31/PECAM-1$^+$ endothelial (N) cell types. The white arrows point to the region depicted in close-up boxes. Scale bars: 100 µm. See also Fig. S1.

mesoderm specific transcript (*Mest*) and *Col1a2* (Fig. S1D), as well as epithelial markers, such *Cdh3*, *Krt7* and *Krt19* (Fig. 1H,K). These cells also expressed *Urk3b*, *Muc16* and *Wt1*, indicating that they represent mesothelium (Mt; Fig. 1D) (Kanamori-Katayama et al., 2011). Cluster 6 represented enteric neural crest-derived progenitors (Ne) expressing *Ret*, *Dlx1*, *Dlx2*, *Ascl1*, *Phox2b*, *Sox10* and *Tubb3* (Fig. 1H,L; Fig. S1D). Hematopoietic cells were separated into two clusters. Cluster 7, representing lympho-myeloid cells (LM), showed expression of *Gpr65*, *Fcer1g*, *Ptprc* (*Cd45*), *Cd44* and *Cd53* (Fig. 1H,M; Fig. S1D). Cluster 8, representing embryonic erythrocytes (Er), was identified by high expression of α- and β-globins (Fig. 1H; Fig. S1D). *Pecam1*-positive endothelial cells did not separate into the individual cluster due to the scarcity of the sequenced cells (only three), yet immunohistochemical analysis showed that this cell type was present within the embryonic stomach mesenchyme (Fig. 1N). Taken together, our single-cell transcriptomic analysis shows that, at E13.5, the embryonic stomach contains three distinct epithelial cell types, three mesenchymal populations (fibroblasts, myofibroblasts and mesothelial cells), enteric neural crest-derived progenitors, endothelial cells, lympho-myeloid cells and erythroid cells. Differentiation of the glandular epithelial cells along three major cell lineages is initiated by this developmental stage.

Axin2⁺ cells are transient embryonic progenitors in forestomach epithelium

A variety of adult stem cells rely on WNT signalling for their maintenance and proliferation (Kretzschmar and Clevers, 2017). During embryogenesis, the WNT pathway is active within intestinal stem cell progenitors (Nigmatullina et al., 2017). To identify embryonic gastric stem cell progenitors, we examined the expression of WNT target genes within the embryonic stomach. RNA *in situ* hybridization (ISH) and scRNA-seq analyses showed that *Axin2* (Lustig et al., 2002) was expressed in the forestomach and corpus epithelium and in the mesenchyme as well as mesothelium at E13.5 (Fig. 2A,B). The expression of *Lgr5* (Barker et al., 2007) was confined to the *Cym*-positive corpus epithelium (Fig. 2A,D). Furthermore, *Lgr5* was weakly expressed in the *Trp63*-positive forestomach epithelium (Fig. 2C) and *Nkx6-2* positive antrum (Fig. 2E).

Axin2⁺ cells constitute a stem cell pool in the adult antrum (Sigal et al., 2017). To assess whether *Axin2*-expressing cells are embryonic gastric progenitors, we analysed their contribution to the adult stomach epithelium by lineage tracing analysis using *Axin2*^{Cre-ERT2} and *Rosa26*^{tdTomato} or *Rosa26*^{lacZ} reporter mice. FACS analysis showed that 9% of stomach epithelial cells were labelled 16 h after a single tamoxifen administration to *Axin2*^{Cre-ERT}/*Rosa26*^{tdTomato} mice at E12.75 (Fig. 2F; Fig. S2A). The proportion of tdTomato-labelled progenies decreased 5.5 times (to 1.6±0.6%) by E18.5 (Fig. S2B). Histological analysis revealed that tdTomato⁺ clones were located in p63-positive forestomach epithelium at E16.5 (Fig. 2G), and they were very rare in ISL1⁺ corpus epithelium or not found in NKX6-3⁺ antral epithelium (Fig. 2H,I). Analysis of the adult stomach at four months of age showed 22±2 clones only in the corpus (Fig. 2J-L). These results indicate that *Axin2* marks a transient population of the embryonic forestomach epithelial progenitors at E13. *Axin2*-expressing cells seldom give rise to the adult stem cells in the corpus epithelium.

Lgr5⁺ cells generate both corpus and forestomach organoids *ex vivo*

Lgr5-expressing cells function as reserve stem cells in the adult corpus epithelium (Leushacke et al., 2017). To study the role of

Lgr5⁺ cells in the embryonic gastric epithelium we followed their fate using *Lgr5*^{EGFP-Cre-ERT} and *Rosa26*^{lacZ} reporter mice. After a single tamoxifen administration at E12.75, only 1±1 *lacZ*⁺ clones were detected in the corpus at four months of age (Fig. 2M). FACS analysis of *Lgr5*^{EGFP-Cre-ERT}/*Rosa26*^{tdTomato} embryos showed that 15.5±1.6% of the gastric epithelial cells were EGFP⁺ at E13.5 (Fig. 3A). Yet, only 1% of them was tdTomato⁺ from E13.5 to E15.5 (Fig. 3B; Fig. S3A). Therefore, conclusions about *in vivo* functions of *Lgr5*⁺ embryonic gastric epithelial cells cannot be made using this *Cre* line.

To evaluate the capacity of *Lgr5*-expressing cells to self-renew and give rise to differentiated cell types, we used an *ex vivo* organoid model system. Lgr5-EGFP⁺EpCAM⁺ and Lgr5-EGFP⁻EpCAM⁺ gastric epithelial cells from *Lgr5*^{EGFP-Cre-ERT} embryos were isolated by FACS at E13.5. We applied the culture conditions used for the mouse adult gastric epithelium, including R-spondin1, noggin, EGF and FGF10 growth factors, Gsk3β kinase inhibitor CHIR-99021 and Rho kinase inhibitor Y27632 (WENRF medium; Schweiger et al., 2018). After 7 days in culture, Lgr5-EGFP⁺ epithelial cells generated 20 times more organoids than either *Lgr5*-negative or *Axin2*⁺ epithelial cells (Fig. 3C-E; Fig. S3B). Three types of organoids were observed: transparent spheroids (50%, Fig. 3E), dark spheroids (15%, Fig. 3E) and a mixture of both (35%, Fig. 3E; Fig. S3C). Both transparent and dark *Lgr5*⁺ spheroids could be maintained for up to five passages in culture (Fig. S3D). In contrast, *Lgr5*⁻-derived transparent organoids were lost after two passages. Accordingly, we detected a high number of apoptotic cells within *Lgr5*⁻-derived organoids (Fig. S3E).

Quantitative reverse-transcription PCR (qRT-PCR) analysis showed that both *Lgr5*⁺- and *Lgr5*⁻-derived organoids expressed gastric marker *Sox2* but were negative for intestinal epithelium markers *Alpi*, *Cdx2*, *Fabp1* and *Fabp2* (Fig. 3F,G). Although the corpus marker *Cym* was highly expressed, the marker for the antral epithelium *Pdx1* was not detected in the *Lgr5*⁺-derived gastric organoids (Fig. 3F). This shows that, consistent with its corpus-specific expression in embryos, *Lgr5*⁺ cells gave rise to the corpus organoids. Moreover, the markers for squamous epithelium, including *Krt5*, *Krt15* and *Trp63* were expressed in the gastric organoids derived from either *Lgr5*⁺ or *Lgr5*⁻ embryonic epithelial cells (Fig. 3H; Fig. S3B) indicating that both types of embryonic epithelial progenitors gave rise also to forestomach organoids.

For further studies, we focused on glandular/transparent organoids not older than 10 days in culture. Expression of the WNT target genes *Axin2* and *Lgr5* was similar between *Lgr5*⁺-, *Lgr5*⁻-derived gastric organoids and the adult corpus or duodenal organoids (Fig. 3I) and was much higher than those in the adult corpus glands. We found that the expression of markers of zymogenic chief cells, including *Mist1*, *Gif* (*Cblif*) and *Pgc*, was more than tenfold higher in organoids derived from *Lgr5*⁺ compared with *Lgr5*⁻ embryonic epithelial cells (Fig. 3J,O-R). This suggests that *Lgr5*⁺ embryonic progenitors are the source of the zymogenic cells in the corpus, as organoids derived from *Lgr5*⁻ cells barely expressed (at levels similar to those found in duodenal organoids) *Mist1*, *Gif* and *Pgc* even in the presence of high WNT signals in culture (Fig. 3J). Similarly, the marker of mucous neck cells *Tff2* showed 65-fold higher expression in *Lgr5*⁺-derived organoids compared with those derived from *Lgr5*⁻ cells (Fig. 3K). Immunostaining confirmed that *Lgr5*⁺-derived organoids contained GS-II lectin-positive mucus neck cells (Fig. 3S,T).

Gastric organoids expressed pit cell markers *Muc5ac* and *Gkn1* (Fig. 3L,U,V), as well as parietal cell marker *Atp4a* (Fig. 3M,W,X), at very low levels of 1000 times less than corpus glands and similar
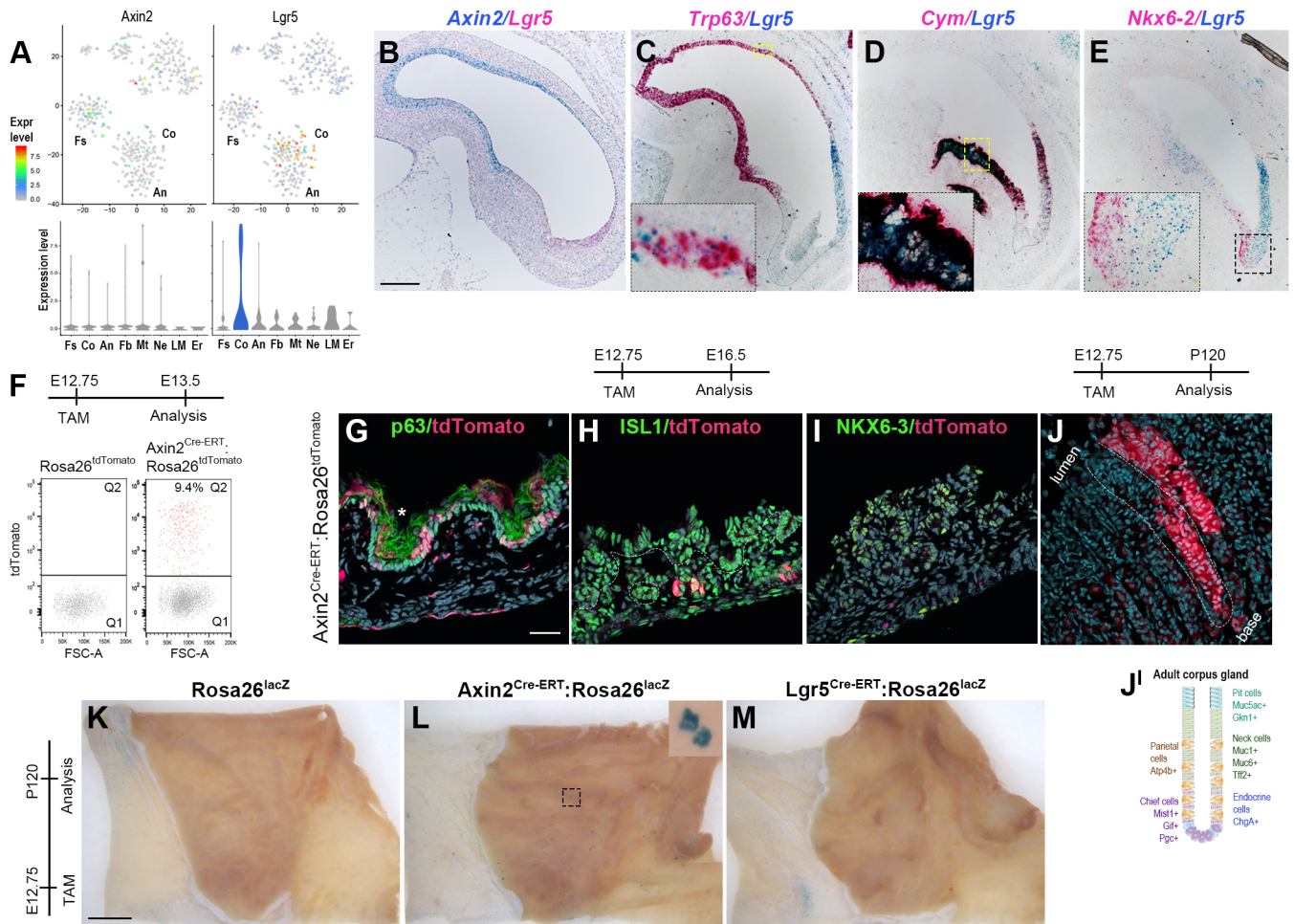
Fig. 2. _Axin2_ marks a transient population of embryonic forestomach epithelium. (A) t-SNE and violin plots of mouse embryonic gastric cells showing expression of _Axin2_ and _Lgr5_ in forestomach (Fs), corpus (Co) and antral (An) epithelium as well as in mesenchymal cells at E13.5. Colour scale reflects normalized expression for each cell in the t-SNE plots and for each cluster in the violin plots. Colour bar: log2(TPM+1). (B) Single-molecule RNA ISH for _Axin2_ (cyan) and _Lgr5_ (magenta) on mouse stomach at E13.5 (n=5). The section was co-stained with haematoxylin. (C-E) Single-molecule RNA ISH for _Trp63/Lgr5_ (C), _Cym/Lgr5_ (D) and _Nkx6-2/Lgr5_ (E) on mouse stomach at E13.5 (n=5). Magnifications of boxed areas show overlap between the expression of _Lgr5_ and the regional markers. (F) Representative FACS plots showing the labelling efficiency of _Axin2_[+] cells 16 h after tamoxifen (TAM) treatment (n=12 embryos analysed). (G-I) Images of E16.5 mouse stomach showing labelled _Axin2_[+] progenies (red) in p63[+] forestomach (G), ISL1^{+} corpus (H) and NKX6-3[+] antral (I) epithelium (n=4 embryos analysed). The asterisk in G indicates squamous epithelial cells with high autofluorescence. (J) Confocal image of _Axin2_[+] progenies (red) in adult corpus epithelium 4 months (P120) after treatment with tamoxifen at E12.75 (n=3 mice analysed). (J′) Schematic for the cellular composition and markers for each cell type of the adult corpus gland. (K-M) Whole-mount view of β-galactosidase-stained _Rosa26_[lacZ] (K), _Axin2_[Cre-ERT]/_Rosa26_[lacZ] (L) and _Lgr5_[EGFP-Cre-ERT]/_Rosa26_[lacZ] (M) stomach four months after a single treatment with TAM at E12.75 (n=5). Scale bars: 100 μm (B-E); 40 μm (G-J); 4 mm (K-M). See also Fig. S2.

to the duodenal organoids, suggesting that only a few cells within the gastric organoids are mature parietal or pit cells. Yet, the expression of _Atp4a_ was higher in organoids derived from _Lgr5_[+] embryonic cells compared with _Lgr5_[-] or adult corpus organoids (Fig. 3M). _ChgB_, a marker for endocrine cells was expressed at low levels in both _Lgr5_[+]- and _Lgr5_[-]-derived organoids (Fig. 3N). In contrast, gastrin (Gast), which is produced by antral endocrine cells in the adult stomach (Willet and Mills, 2016) was detected only in organoids derived from _Lgr5_[-] cells (Fig. 3N), which is consistent with their antral origin. In summary, these data demonstrate that _Lgr5_[+] embryonic epithelial cells have much higher capacity than _Lgr5_[-] cells to generate corpus organoids _ex vivo_. _Lgr5_[+] progenitors retain self-renewal and differentiation capacity _ex vivo_ and give rise to the zymogenic chief cell lineage. Although WNT target genes could be activated in _Lgr5_[-]-derived organoids, chief cell markers were not expressed in these organoids.

WNT signalling promotes differentiation along the zymogenic chief cell lineage but blocks mucous pit cell specification

Differentiation of the gastric epithelium commences around E13.5 and is accompanied by activation of the chief and parietal cell-specific genes (Willet and Mills, 2016). To identify signals that initiate the transition of embryonic gastric progenitors towards three major cell lineages, we looked for the expression of factors controlling cell fate decisions. scRNA-seq and RNA ISH analyses of the embryonic stomach at E13.5 revealed that _Wnt5a_ was expressed in the mesenchyme and at low levels in a subset of epithelial cells (Fig. 4A,B). _Wnt5b_ was detected in the forestomach and corpus epithelium as well as in a few mesenchymal cells, with highest expression in the mesothelium (Fig. 4A,C). Furthermore, both R-spondin1 (_Rspo1_) and R-spondin3 (_Rspo3_), which enhance WNT signalling, were highly expressed in the mesothelium and subpopulations of mesenchymal cells (Fig. 4A,D,E).
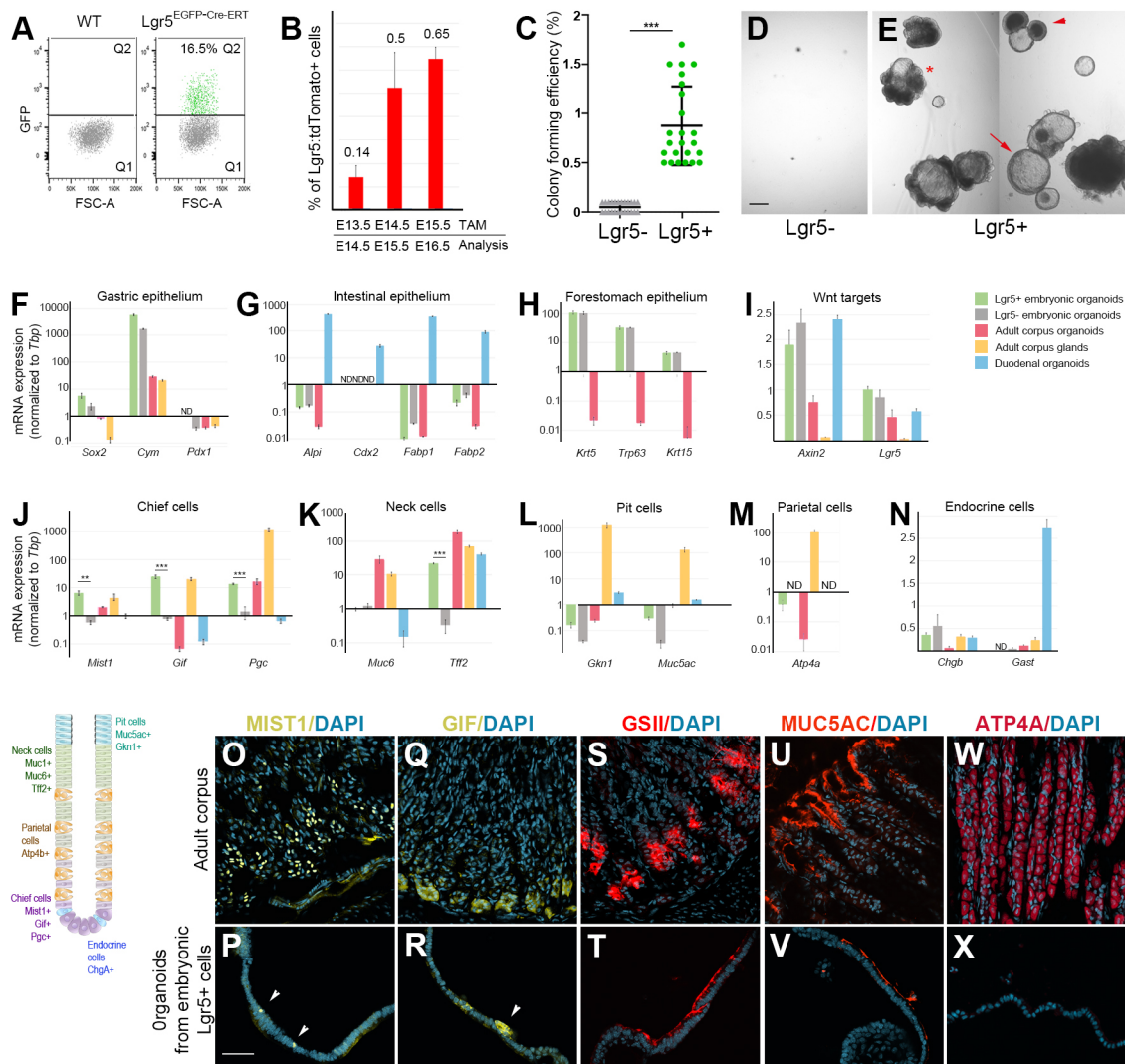
Fig. 3. *Lgr5*^{+} embryonic progenitors generate both forestomach and corpus organoids. (A) Representative FACS plot showing strategy to isolate Lgr5-EG[+] EpCAM[+] (green) and Lgr5-EGFP[-]EpCAM^{+} cells (grey) for *ex vivo* organoid culture at E13.5 (*n*=24). (B) Quantification of Lgr5-EGFP[+]:tdTomato[+]EpCAM^{+} cells by FACS one day after a single treatment with TAM at different embryonic stages (*n*=5). (C) Colony-forming efficiency of Lgr5-EGFP[-]EpCAM[+] and Lgr5-EGFP[+] EpCAM^{+} cells isolated by FACS at E13.5 (*n*=24). (D,E) Gastric organoids from Lgr5-EGFP[-]EpCAM[+] and Lgr5-EGFP[+]EpCAM[+] embryonic stomach epithelium in 7-day culture. Note heterotopic colony formation from *Lgr5*^{+} cells. Arrow, corpus organoid; arrowhead, forestomach organoid; asterisk, mixed organoid. (F-N) qRT-PCR analysis for expression of the indicated marker genes in organoids derived from *Lgr5*^{+} embryonic epithelial cells (green), *Lgr5*^{-} embryonic epithelial cells (grey), adult corpus organoids (red), adult corpus glands (yellow) and adult duodenum organoids (blue). *Tbp* expression was used as a normalizing control (*n*=3). (O-X) Schematic of the adult corpus gland showing the cellular composition and markers for each cell type. Immunostaining of sections of adult corpus and organoids derived from *Lgr5*^{+} embryonic cells show MIST1^{+} chief cells (yellow, O,P), GIF^{+} chief cells (yellow, Q,R), GSII[+] mucous neck cells (red, S,T), MUC5AC^{+} mucous pit cells (red, U,V), and ATP4a^{+} parietal cells (red, W,Y) (*n*=3). Nuclei were stained with DAPI (blue). Error bars indicate s.d. ***$P<0.001$ and **$P<0.01$ by two-tailed unpaired Student's *t*-test. Scale bars: 1 mm (D,E); 50 μm (O,X). See also Fig. S3.

To investigate the function of WNT signalling in the embryonic stomach, we inhibited the activity of Porcupine, which is essential for the secretion of WNTs (Tanaka et al., 2002). At 16 h after an application of Wnt-C59 inhibitor, the expression of the WNT target gene *Axin2* was reduced fourfold compared with vehicle-treated embryos (Fig. 4F; Fig. S4A). The expression of *Lgr5* was reduced by 70% (Fig. 4F,L,M; Fig. S4B,C). Inhibition of WNT signalling led to a strong loss of zymogenic chief cell markers *Gif* (25-fold) and *Pgc* (eightfold) (Fig. 4G,L,M; Fig. S4D,E), indicating that WNTs are required for the differentiation of the embryonic gastric progenitors along zymogenic cell lineage. Moreover, *Atp4a* was significantly downregulated (fourfold) in Wnt-59C-treated embryos (Fig. 4H). WNT signalling is essential for specification of the corpus epithelium during embryogenesis (McCracken et al., 2017).

Accordingly, we detected a significant reduction in *Cym* expression in embryos treated with Wnt-59C compared with controls (Fig. 4H; Fig. S4B,D,F). Therefore, the reduction of *Atp4a* expression could be secondary to the 'reduced' corpus identity in WNT-deficient embryos.

Strikingly, *Muc5ac* was induced over 3000-fold upon loss of WNT signalling in the embryonic stomach (Fig. 4I), indicating that WNTs negatively control the differentiation of gastric progenitors along the pit cell lineage. *Muc5ac* was activated in both *Cym*[+] corpus and *Nkx6-2*[+] antrum epithelium (Fig. 4N-O″; Fig. S4F-I).

Depletion of WNT signals did not induce apoptosis (Fig. S4K,L) or affect cell proliferation in the epithelium (Fig. S4S-T) but blocked it in the mesenchyme (Fig. S4S′-T′), which was consistent with the smaller size of the stomach (Fig. 4L-O). However, prolonged
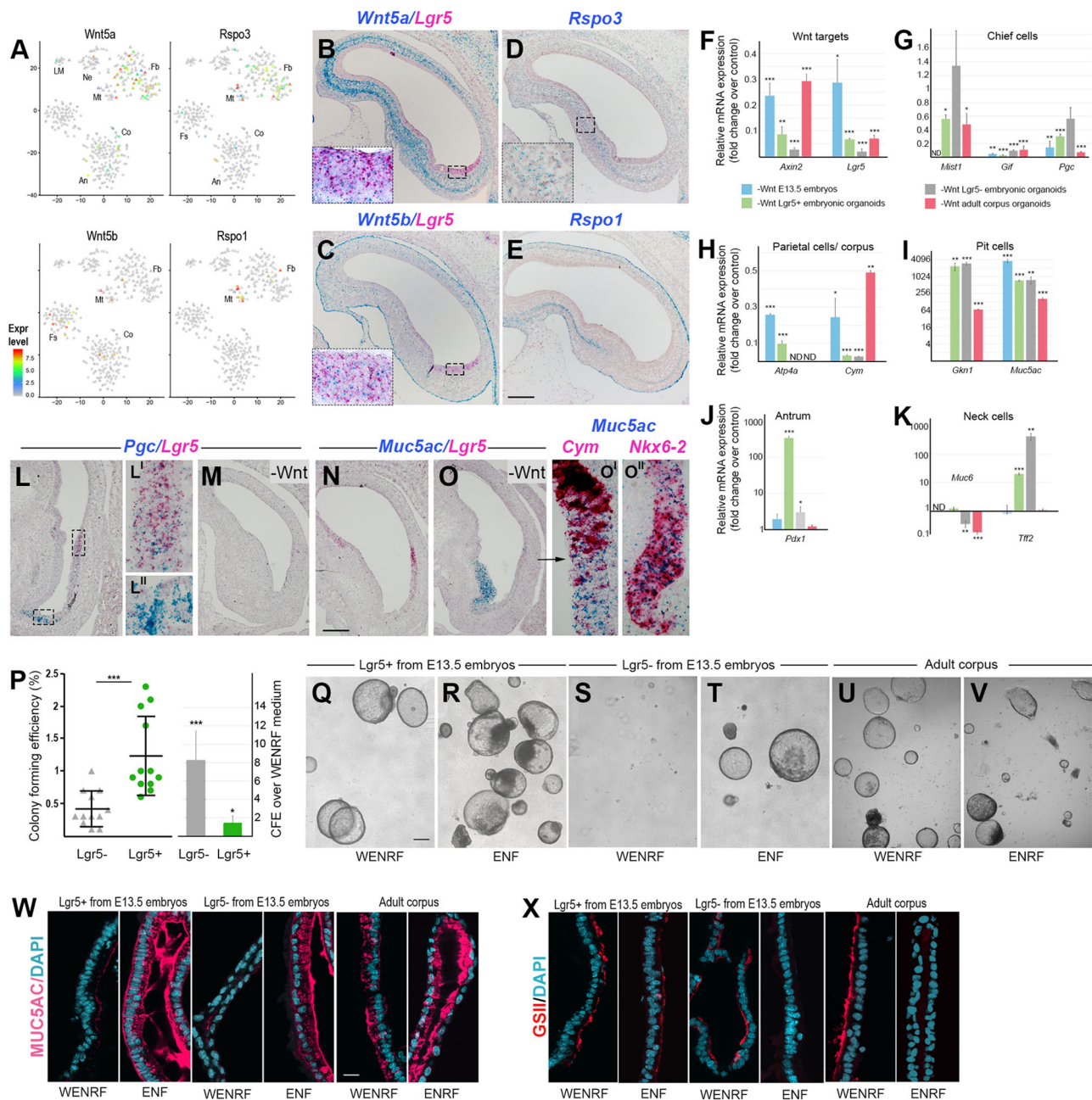
Fig. 4. Functions of WNT signalling in the embryonic gastric epithelium. (A) t-SNE plots of mouse embryonic gastric cells. Single cells coloured by expression of *Wnt5a*, *Wnt5b*, *Rspo3* and *Rspo1* in forestomach (Fs), corpus (Co) and antral (An) epithelium, fibroblast (Fb), mesothelial (Ms), enteric neural (Ne) and lympho-myeloid (LM) cell lineages. Colour bar: log2(TPM+1). (B-E) smRNA ISH for *Wnt5a/Lgr5* (B), *Wnt5b/Lgr5* (C), *Rspo3* (D) and *Rspo1* (E) on mouse stomach at E13.5 (*n*=5). (F-K) qRT-PCR analysis showing expression of the indicated markers in stomach epithelium of the embryos treated for 16 h with WNT inhibitor Wnt-59C compared with vehicle-treated controls (blue) in *Lgr5*⁺-derived organoids (green) and *Lgr5*⁻-derived organoids (grey) cultured for 7 days in ENF medium compared with WENRF, and in adult corpus organoids cultured for 48 h without or with Gsk3β inhibitor (pink) (*n*=3). *Tbp* expression was used as a normalizing control. (L-O″) smRNA ISH showing expression of the indicated transcripts on E13.5 stomach from wild-type (L,N) and Wnt-59C treated (M,O) embryos (*n*=3). Magnification of boxed area in L′ shows the overlap between *Pgc* and *Lgr5* expression in the control embryo. (O′,O″) Magnifications from Fig. S4H,I for *Muc5ac/Cym* (O′) and *Muc5ac/Nkx6-2* (O″) on E13.5 stomach from Wnt-59C-treated embryos (*n*=3). (P) Colony-forming efficiency of *Lgr5*-EGFP⁻EpCAM⁺ and Lgr5-EGFP⁺EpCAM⁺ cells isolated by FACS at E13.5 and grown in ENF medium (left). Colony-forming efficiency of Lgr5-EGFP⁻EpCAM⁺ and Lgr5-EGFP⁺EpCAM⁺ cells grown in ENF versus WENRF medium (right) (*n*=12). (Q-V) Representative images of organoids derived from *Lgr5*⁺ (Q,R) and *Lgr5*⁻ embryonic epithelium (S,T) cultured for 7 days either in WENRF or ENF medium, and adult corpus organoids cultured for 48 h either without (ENRF) or with Gsk3β inhibitor (U,V) (*n*=12). (W,X) Immunostaining of organoids derived from *Lgr5*⁺ or *Lgr5*⁻ cells or adult corpus labelled for MUC5AC showing mucous pit cells (pink, W), GSII showing mucous neck cells (red, X) cultured in WENRF, ENF or ENRF medium, (*n*=3). Nuclei stained with DAPI (blue). Error bars indicate s.d. ***P<0.001, **P<0.01 and *P<0.05 by two-tailed unpaired Student's *t*-test. Scale bars: 100 μm (B-E); 75 μm (L-O); 0.3 mm (Q-V); 25 μm (W,X); 15 μm (L′-M′,O′,O″). See also Fig. S4.

inhibition of WNT signalling leads to embryonic lethality. Therefore, to test the effects of WNT depletion on embryonic gastric progenitors and further define functional differences between *Lgr5*⁺ and *Lgr5*⁻ gastric epithelial cells, we isolated those cells from *Lgr5*^*EGFP−Cre-ERT* embryos by FACS at E13.5 and cultured them in the absence of the Gsk3β kinase inhibitor

CHIR-99021 and R-Spondin1 (ENF medium). Surprisingly, both $Lgr5^+$ and $Lgr5^-$ cells generated significantly more organoids than those grown in full or corpus medium (Fig. 4P-T). Again, $Lgr5^+$ epithelial cells displayed three times higher colony-forming capacity than $Lgr5^-$ cells (Fig. 4P,R,T). Similar to the situation in full WENRF culture conditions, $Lgr5^-$-derived organoids could not be maintained in ENF culture for more than three passages as a result of apoptosis (Fig. S4M-P,U-X), whereas $Lgr5^+$-derived organoids could be maintained for at least five passages. qRT-PCR analysis showed that the expression of corpus marker *Cym* was reduced 30-fold and that the expression of antrum marker *Pdx1* was upregulated in the embryonic organoids cultured in the absence of WNT signals (Fig. 4H,J), indicating that both $Lgr5^+$ and $Lgr5^-$ embryonic cells generated antral organoids in ENF medium.

Similar to the results for embryos, expression of WNT target genes *Axin2* and *Lgr5* was downregulated in $Lgr5^+$- and $Lgr5^-$-derived embryonic organoids and in adult corpus organoids in the absence of WNT signalling (Fig. 4F,U,V). Chief cell markers *Mist1* and *Pcg* were significantly downregulated in $Lgr5^+$ and adult corpus organoids (Fig. 4G). Moreover, the parietal cell marker *Atp4a* (corpus specific) was downregulated in $Lgr5^+$-derived organoids (Fig. 4H).

On the other hand, *Muc5ac* was strongly induced in $Lgr5^+$, $Lgr5^-$ and adult organoids (Fig. 4I,W). The loss of WNT signalling had different effects on the expression of neck cell markers *Muc6* and *Tff2* only in the organoids but not in embryos (Fig. 4K,X), which could be due to the *ex vivo* culture conditions. The different behaviour of *Muc6* and *Tff2* is consistent with the results of a study showing that *Muc6* and *Tff2* are expressed in different populations of mucous cells in the adult stomach epithelium (Bockerstett et al., 2020). Thus, we conclude that WNT signalling controls patterning of the embryonic stomach and promotes corpus identity within the epithelium at least until E13.5. WNT signals enhance differentiation of gastric progenitors towards the zymogenic lineage but severely inhibit their commitment to the pit cell lineage in both corpus and antrum. Finally, $Lgr5^+$ embryonic epithelial cells have a higher capacity than $Lgr5^-$ cells to generate antral organoids *ex vivo*.

BMP signalling controls differentiation of gastric progenitors along parietal and pit cell lineages

In the adult corpus, BMP signalling blocks differentiation of gastric progenitors along the mucous neck and pit cell lineages and is required for the generation of parietal cells (Maloum et al., 2011). Several BMP genes were expressed in the embryonic stomach at E13.5. Whereas *Bmp4* was restricted to the subepithelial mesenchyme (Fig. 5A,B), *Bmp1* and *Bmp7* were broadly expressed in both the epithelial and mesenchymal cells (Fig. S5A). In agreement with previous studies, *Bmpr1a* was ubiquitously expressed in the embryonic stomach (Fig. 5A,C).

To determine the role of BMP signalling in the maintenance and specification of the embryonic gastric epithelial progenitors we blocked the activity of BMPR1A using LDN193189 inhibitor (Fig. S5B,C). Inhibition of BMP signalling for 16 h induced the expression of *Lgr5* (3.6-fold) but not *Axin2* (Fig. 5D). $Lgr5^+$ cells were confined to Cym^+ corpus epithelium in LDN193189-treated embryos, as in controls (Fig. S5D-E′). However, the number of Lgr5-EGFP$^+$ cells was significantly increased, as revealed by FACS analysis (Fig. 5E). This indicates that BMP signalling restricts the number of $Lgr5^+$ embryonic epithelial cells.

We also found that the expression of *Muc5ac* was strongly upregulated (9000-fold) in LDN193189-treated embryos compared with controls (Fig. 5F,L-O′), indicating that BMP signalling inhibits

differentiation of embryonic gastric progenitors along the pit cell lineage. *Muc5ac*-expressing cells were located in both *Cym*-positive corpus epithelium (Fig. 5L-M′) and *Nkx6-2*-positive antrum epithelium (Fig. 5N-O′). Of note, the expression of *Nkx6-2* was significantly reduced in LDN193189-treated embryos compared with controls (Fig. 5K,N-O′), indicating that BMP signals are necessary for either the expression of this gene or the specification of the embryonic gastric epithelium towards antral fate.

The expression of parietal cell marker *Atp4a* was reduced sevenfold upon inhibition of BMP signalling (Fig. 5G,P-Q′), indicating that BMP signalling is required for specification of embryonic gastric progenitors along parietal cell lineage. Moreover, chief cell marker *Gif* (Fig. 5H) and neck cell marker *Tff2* (Fig. 5I) were significantly downregulated (two- to threefold) upon inhibition of BMP signalling. Finally, the expression of endocrine cell marker *ChgB* was significantly downregulated upon loss of BMP signalling (Fig. 5J), which is consistent with the requirement of BMP signals for the differentiation of the entero-endocrine cells (Beumer et al., 2018).

We next tested the effects of BMP signalling in organoid cultures. Lgr5-EGFP$^+$EpCAM$^+$ and Lgr5-EGFP$^-$EpCAM$^+$ gastric epithelial cells from *Lgr5$^{EGFP-Cre-ERT}$* embryos and organoids derived from adult corpus were cultured in the absence of the BMP antagonist noggin (WERF medium). The colony-forming efficiency was improved almost ten times for $Lgr5^+$ cells and over 100 times for $Lgr5^-$ cells plated in WERF medium (Fig. 5R-V). Furthermore, $Lgr5^-$ cells displayed significantly higher colony-forming capacity than $Lgr5^+$ cells in the presence of BMP signals (Fig. 5R). Both types of organoids could be maintained for at least five passages in culture. Consistent with improved clonogenic capacity, we detected a higher number of Ki67$^+$ cells in $Lgr5^+$ cells, together with less apoptotic cells in $Lgr5^-$-derived organoids cultured in WERF medium compared to those cultured in WENRF (Fig. 5Y,Z; Fig. S5F-I).

Inhibition of BMP signalling led to 50-fold upregulation of the corpus marker *Cym* and 100-fold downregulation of the antral markers *Pdx1* and *Nkx6-2* in $Lgr5^+$-derived organoids (Fig. 5G,K). The same changes were observed in $Lgr5^-$-derived organoids and adult corpus organoids, yet to a lower degree (Fig. 5G,K). This indicates that BMP signals promote antral fate in gastric epithelial cells even in the presence of high WNT signalling.

Similar to the results in embryos, inhibition of BMP signalling induced the expression of *Lgr5* in both $Lgr5^+$- and $Lgr5^-$-derived organoids (Fig. 5D). Furthermore, the expression of *Muc5ac* was increased 15-fold upon inhibition of BMP signalling in adult corpus organoids (Fig. 5F,AB). BMP signals were also required for the expression of neck cell marker *Tff2* (Fig. 5I) in both $Lgr5^+$- and $Lgr5^-$-derived organoids and *Muc6* in $Lgr5^+$ only (Fig. 5I,AA; Fig. S5J-M). In contrast to the results in embryos, pit cells marker *Muc5ac* was downregulated (Fig. 5F; Fig. S5N-Q), parietal cell marker *Atp4a* (Fig. 5G) and entero-endocrine cell marker *ChgB* (Fig. 5J) were upregulated upon inhibition of BMP signalling in $Lgr5^+$-derived organoids. The most parsimonious explanation for this discrepancy is that we studied the effects of BMP signal depletion in both corpus and antral epithelium in embryos, whereas *ex vivo* we compare antrum-like organoids grown in WERF medium with corpus-like organoids grown in WERNF medium. Thus, BMP signals are sufficient to promote antral fate in *ex vivo* organoid culture. Furthermore, BMP signalling limits the number of $Lgr5^+$ epithelial cells as well as their differentiation along the mucous pit cell lineages but it supports their differentiation along the parietal cell lineage.
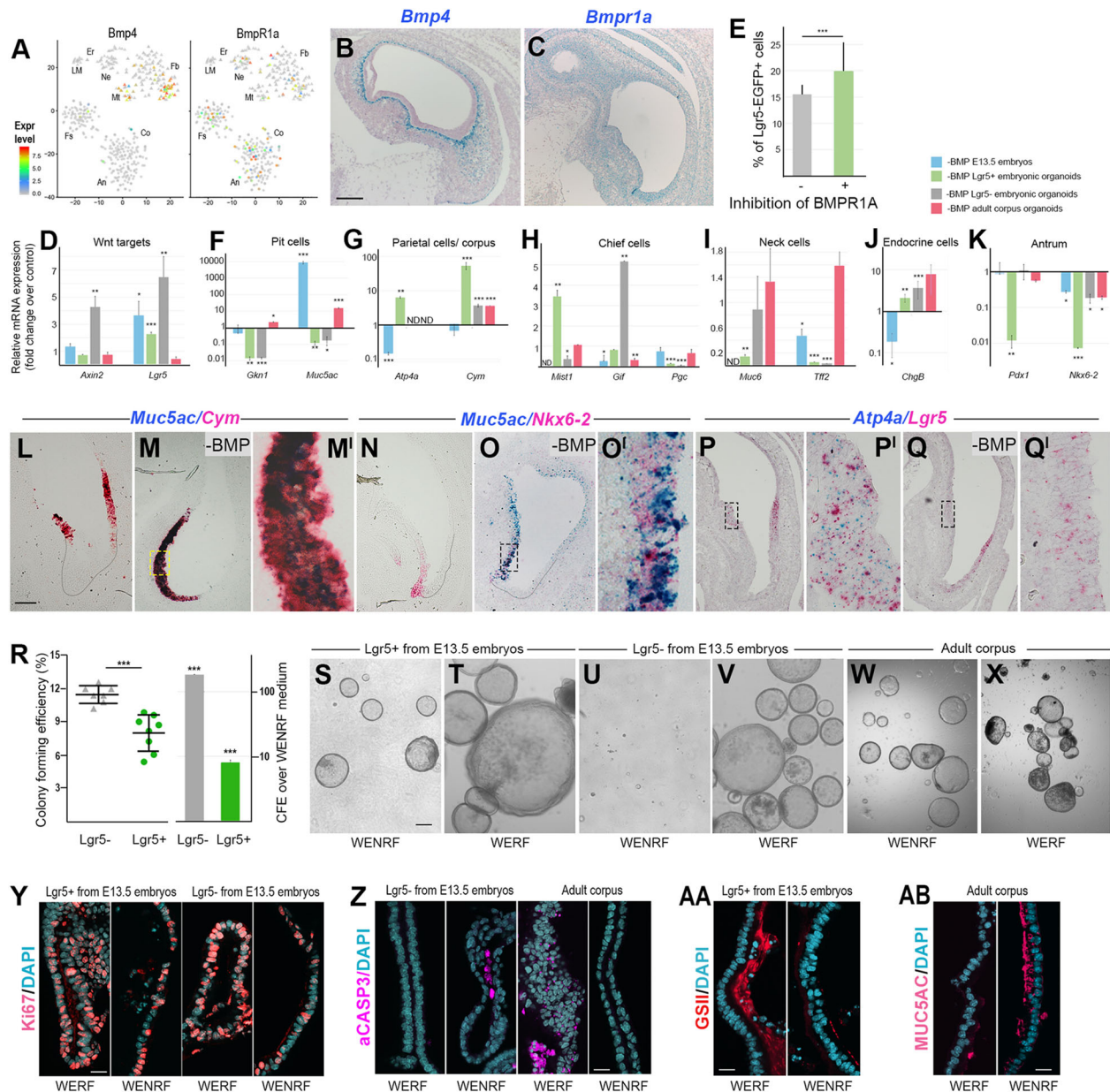
Fig. 5. BMP signalling inhibits differentiation of embryonic gastric progenitors along the pit cell lineage. (A) t-SNE plots of mouse embryonic gastric cells. Single cells coloured by expression of *Bmp4* and *BmpR1a* in forestomach (Fs), corpus (Co) and antral (An) epithelium, fibroblast (Fb), mesothelial (Ms), enteric neural (Ne), lympho-myeloid (LM) and erythroid (Er) cell lineages. Colour bar: log2(TPM+1). (B,C) smRNA ISH for *Bmp4* (B) and *BmpR1a* (C) on mouse stomach at E13.5 (*n*=5). The sections were co-stained with haematoxylin. (D,F-K) qRT-PCR analysis showing expression of the indicated markers in stomach epithelium of embryos treated for 16 h with BMP receptor 1A inhibitor LDN193189 compared with vehicle-treated controls (blue), in *Lgr5*⁺- (green) and *Lgr5*⁻-derived organoids (grey) cultured for 7 days, and in adult corpus organoids cultured for 48 h in WERF medium compared with WENRF (pink) (*n*=3). *Tbp* expression was used as a normalizing control. (E) FACS quantification of Lgr5-EGFP⁺EpCAM⁺ gastric epithelial cells from LDN193189 treated and control embryos at E13.5 (*n*=19). (L-Q′) smRNA ISH showing expression of the indicated transcripts on E13.5 stomach from wild type (L,N,P) and LDN193189-treated (M,O,Q) embryos (*n*=3). M′-Q′ show magnified views of the boxed areas. (R) Colony-forming efficiency of Lgr5-EGFP⁻EpCAM⁺ and Lgr5-EGFP⁺EpCAM⁺ cells isolated by FACS at E13.5 and cultured in WERF medium (left). Colony-forming efficiency of Lgr5-EGFP⁻EpCAM⁺ and Lgr5-EGFP⁺EpCAM⁺ cells cultured in WERF versus WENRF medium (right) (*n*=8). (S-X) Representative images of organoids derived from *Lgr5*⁺ embryonic epithelium (S,T) and *Lgr5*⁻ embryonic epithelium (U,V) cultured for 7 days, and adult corpus organoids cultured for 48 h (W,X) either in the absence or in the presence of noggin (*n*=8). (Y-AB) Immunostaining of organoids derived from embryonic *Lgr5*⁺ or *Lgr5*⁻ cells or adult corpus labelled for KI67 showing proliferating cells (red, Y), aCASP3 showing apoptotic cells (magenta, Z), GSII showing mucous neck cells (red, AB) and MUC5AC showing mucous pit cells (pink, AB) cultured in WENRF or WERF medium (*n*=3). Nuclei stained with DAPI (blue). Error bars indicate s.d. ***P<0.001, **P<0.01 and *P<0.05 by two-tailed unpaired Student's *t*-test. Scale bars: 100 µm (B,C,L-Q); 15 µm (M′,O′-Q′); 0.3 mm (S-X); 25 µm (Y-AB). See also Fig. S5.

Notch signalling blocks differentiation of embryonic gastric progenitors

Notch signalling controls adult gastric stem/progenitor cell proliferation (Kim and Shivdasani, 2011; Demitrack et al., 2017).

In the embryonic stomach, *Notch1* and *Notch2* receptors were broadly expressed in both the epithelium and mesenchyme (Fig. 6A,B; Fig. S6A). *Notch3* and *Notch4* were expressed in less than 10% of sequenced cells. The ligand *Jag1* was expressed in the

highest number of cells according to scRNA-seq analysis (Fig. 6A). RNA ISH confirmed that *Jag1* transcripts were present in the mesenchyme and at very low levels in epithelial cells (Fig. 6B). Finally, the Notch target gene *Hes1* was expressed ubiquitously in the embryonic stomach, indicative of active signalling (Fig. S6A).

To explore the functions of Notch signalling in the embryonic gastric progenitors we applied the γ-secretase inhibitor RO4929097, which blocks the processing of Notch receptors (Fig. S6B,C). At 16h after RO4929097 administration, pit cell marker *Muc5ac* was induced 17,000-fold (Fig. 6C). *Muc5ac* was activated in both *Cym*-positive corpus (Fig. 6K-L′) as well as in *Nkx6-2*-positive antral epithelium (Fig. 6M-N′). Notch inhibition also increased the expression of chief and neck cell markers *Pgc* (sixfold) and *Tff2* (threefold) in the embryonic stomach at E13.5 (Fig. 6D,E). Although the expression of *Pgc* was not changed in *Lgr5*⁺ corpus epithelium (Fig. 6O-P′; Fig. S6D-E′), it was higher in the *Nkx6-2*-positive antral epithelium (Fig. 6Q-R′). Moreover, *Tff2*-positive cells were detected in the antral epithelium upon inhibition of Notch signals (Fig. 6S-T′). Furthermore, *Lgr5* but not *Axin2* was upregulated upon loss of Notch signalling in the embryonic stomach (Fig. 6F,G). Higher expression of *Lgr5* was detected in the *Nkx6-2*-negative cells (Fig. 6U-V″; Fig. S6F-G′) of RO4929097-treated embryos compared with controls. These data indicate that, during embryogenesis, Notch signalling has different functions in the corpus versus antrum. Finally, both parietal cell marker *Atp4a* (Fig. 6H) and endocrine cell marker *ChgB* (Fig. 6I) were upregulated upon loss of Notch signalling, suggesting that Notch signalling blocks differentiation of the gastric embryonic progenitors along all secretory lineages.

Next, we analysed the effects of Notch inhibition on organoids derived from *Lgr5*⁺ and *Lgr5*⁻ embryonic epithelial cells, as well as from the adult corpus. Both *Lgr5*⁺ and *Lgr5*⁻ cells generated significantly more organoids in a medium supplemented with Notch inhibitor RO4929097 compared with those grown in WENRF medium only (Fig. 6W-AA). *Lgr5*⁺ and *Lgr5*⁻ epithelial cells had the same colony-forming capacity (Fig. 6W). Whereas *Lgr5*⁻-derived organoids could be maintained in culture for at least five passages, *Lgr5*⁺-derived organoids were lost after two passages in the presence of RO4929097. Further analysis revealed that blocking of Notch signalling led to apoptosis in *Lgr5*⁺-derived organoids (Fig. 6AD; Fig. S6H-K). The same effect was observed for the organoids derived from the adult corpus (Fig. 6AD). Moreover, proliferation was reduced in both E13.5 embryos and *Lgr5*⁺-derived organoids upon inhibition of Notch signalling (Fig. 6AE; Fig. S6L,M) but not in *Lgr5*⁻-derived or adult corpus organoids (Fig. S6N-Q).

qRT-PCR analysis showed that the expression of *Cym* was strongly downregulated in organoids derived from *Lgr5*⁺ (eightfold) and *Lgr5*⁻ (40-fold) embryonic epithelial cells (Fig. 6H). In contrast, *Pdx1* expression was upregulated in organoids derived from *Lgr5*⁺ (40-fold) and *Lgr5*⁻ (fivefold) embryonic epithelial cells (Fig. 6J) upon loss of Notch signalling. These data indicate that Notch signalling is required for the maintenance of corpus identity in *ex vivo* cultures.

Like in embryos, Notch inhibition induced expression of pit cell markers *Gkn1* and *Muc5ac* 10- to 100-fold in *Lgr5*⁺- and *Lgr5*⁻-derived organoids, respectively (Fig. 6C,AF). Chief cell marker *Pgc* was upregulated in *Lgr5*⁻-derived and adult organoids (Fig. 6D). Furthermore, the expression of neck cell markers *Muc6* and *Tff2* was upregulated in *Lgr5*⁺- and *Lgr5*⁻-derived organoids (Fig. 6E,AG). In contrast to the results in embryos, inhibition of Notch signalling led to downregulation of *Atp4a* (Fig. 6H), *ChgB* (Fig. 6I), *Axin2* and *Lgr5* (Fig. 6F) in *Lgr5*⁺- and *Lgr5*⁻-derived organoids. These expression

changes reflect the corpus (WENRF) versus antrum identity (WENRF plus RO4929097) of the organoids. Inhibition of Notch signalling in the adult corpus organoids affected the expression of *Cym* similarly as in organoids derived from the embryos (Fig. 6H) but did not significantly change the expression of any other tested gene (Fig. 6C-J; Fig. S6R-U). In summary, Notch signalling negatively regulates the expression of *Lgr5* in corpus epithelial cells. It blocks differentiation of the embryonic gastric epithelium towards pit cell and endocrine cell lineages. Notch signals inhibit differentiation towards chief and neck cells in the antral epithelium. Finally, Notch signals promote corpus identity in *ex vivo* organoid cultures.

DISCUSSION
In this study, we show that WNT and Notch signals are necessary for the maintenance of the corpus identity, whereas BMP signals are sufficient to promote the antrum identity of the embryonic gastric epithelial cells (Fig. 7). Embryonic *Lgr5*⁺ cells are functionally different from *Lgr5*⁻ cells in their capacity to specify towards chief or parietal cell lineages *ex vivo*. *In vivo*, *Lgr5*⁺ cells require WNT signals for their maintenance. In contrast, BMP and Notch signals limit the number of *Lgr5*⁺ cells during embryogenesis. We also found that WNT signals are required for the differentiation of the embryonic epithelium along the zymogenic cell lineage, whereas BMP signals are required for the differentiation of the gastric epithelium along the parietal cell lineage. In contrast, they block differentiation of the embryonic progenitors along the pit lineage. Finally, inhibition of Notch signalling leads to differentiation of the embryonic gastric progenitors along all secretory lineages.

Key transcription factors and morphogens that instruct early specification and ontogenesis of the foregut was defined in earlier studies (Willet and Mills, 2016). However, factors controlling specification of the gastric epithelial cells along chief, parietal and pit cells lineages during embryogenesis remained largely unknown. We also lacked knowledge about the identity and diversity of the embryonic gastric epithelial progenitors. We used scRNA-seq to define cell types and their differentiation states in the embryonic stomach at E13.5. Cells expressing mucous neck/chief, parietal and pit lineage markers are present at this developmental stage. On the other hand, entero-endocrine cells were not detected. The forestomach epithelium is composed of both *Trp63*⁺ stem cells and differentiated *Krt15*⁺ progenies. This indicates that differentiation of the gastric epithelium is initiated by E13.5, implying that signals and factors controlling the differentiation of the epithelial progenitors could be identified at this stage.

We found that morphologically identical embryonic gastric epithelial cells are molecularly and functionally heterogeneous. For example, *Axin2* transcripts could be detected within all three domains of the embryonic stomach. In contrast, *Lgr5* is highly expressed in the embryonic corpus epithelium. *Axin2*⁺ cells form transient clones only in the forestomach epithelium but do not contribute to the adult forestomach epithelial stem cells. A minuscule fraction of cells expressing *Axin2* contributes to the adult corpus stem cell pool. Consistently, *Axin2*⁺ cells display a low colony-forming efficiency in *ex vivo* organoid cultures. This suggests that the majority of *Axin2*⁺ cells represent differentiated progenies at E13.5.

Lgr5⁺ cells generate corpus organoids *ex vivo* 20-fold more efficiently than *Axin2*⁺ or *Lgr5*⁻ cells. Moreover, *Lgr5*⁺ cells have higher efficiency than *Lgr5*⁻ cells to generate antral organoids in WNT-free culture conditions. Importantly, embryonic *Lgr5*⁺ cells are functionally different from *Lgr5*⁻ cells in their capacity to specify towards chief or parietal cell lineages *ex vivo*. Only
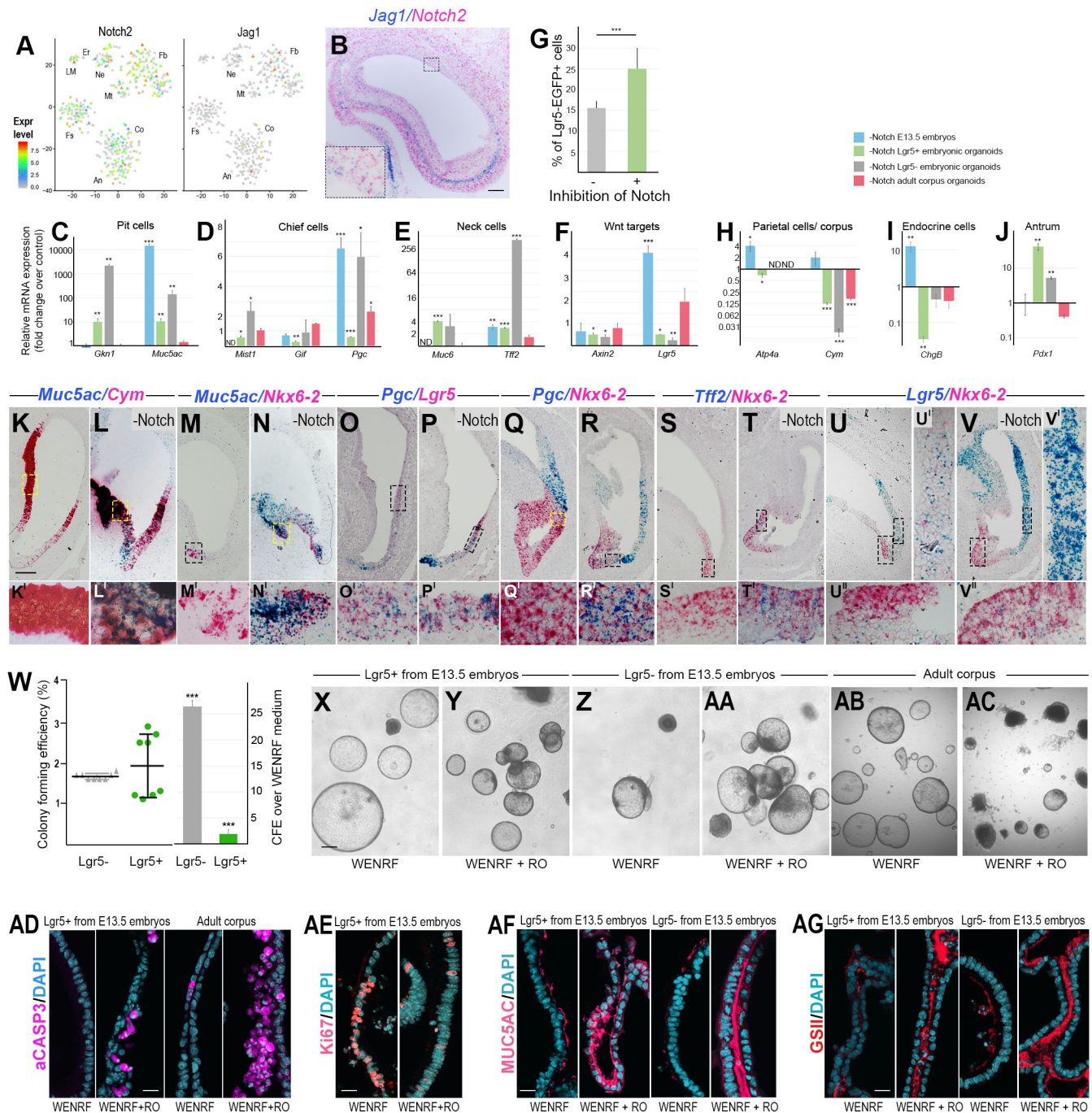
DEVELOPMENT

Fig. 6. Notch inhibition enhances the differentiation of the embryonic gastric progenitors. (A) t-SNE plots of mouse embryonic gastric cells. Single cells coloured by expression of *Notch2* and *Jag1* in forestomach (Fs), corpus (Co) and antral (An) epithelium, in fibroblast (Fb), mesothelial (Ms), enteric neural (Ne), lympho-myeloid (LM) and erythroid (Er) cell lineages. Colour bar: log2(TPM+1). (B) smISH for *Notch2*/*Jag1* on mouse stomach at E13.5 (*n*=5). (C-F,J) qRT-PCR analysis showing expression of the indicated markers in stomach epithelium of embryos treated for 16 h with Notch inhibitor RO4929097 compared with vehicle-treated controls (blue), in *Lgr5*+- (green) and *Lgr5*−-derived organoids (grey) cultured for 7 days, and in adult corpus organoids cultured for 48 h in the presence of RO4929097 compared with DMSO control (pink) (*n*=3). *Tbp* expression was used as a normalizing control. (G) FACS quantification of Lgr5-EGFP+EpCAM+ gastric epithelial cells from RO4929097-treated and control embryos at E13.5 (*n*=11). (K-V″) smRNA ISH showing expression of the indicated transcripts on E13.5 stomach from control and RO4929097-treated (-Notch) embryos (*n*=3). K′-V″ show magnified views of the boxed areas. (W) Colony-forming efficiency of Lgr5-EGFP−EpCAM+ and Lgr5-EGFP+EpCAM+ cells isolated by FACS at E13.5 and cultured in WERNF medium in the presence of RO4929097 (left). Colony-forming efficiency of Lgr5-EGFP−EpCAM+ and Lgr5-EGFP+EpCAM+ cells cultured in the presence of either RO4929097 or DMSO (right) (*n*=8). (X-AC) Representative images of organoids derived from *Lgr5*+ (X,Y) and *Lgr5*− embryonic epithelium (Z,AA) cultured for 7 days, and adult corpus organoids cultured for 48 h in the presence of either RO4929097 or DMSO (AB,AC) (*n*=8). (AD-AG) Immunostaining of organoids derived from embryonic *Lgr5*+ and *Lgr5*− cells or adult corpus labelled for aCASP3 showing apoptotic cells (magenta, AD), KI67 showing proliferating cells (red, AE), MUC5AC showing mucous pit cells (pink, AF) and GSII showing mucous neck cells (red, AG) cultured either with DMSO (WENRF) or with Notch inhibitor RO4929097 (WENRF+RO) (*n*=3). Nuclei stained with DAPI (blue). Error bars indicate s.d. ***P<0.001, **P<0.01 and *P<0.05 by two-tailed unpaired Student's *t*-test. Scale bars: 100 μm (B,K-V); 15 μm (K′-V″); 0.3 mm (X-AC); 25 μm (AD-AG). See also Fig. S6.
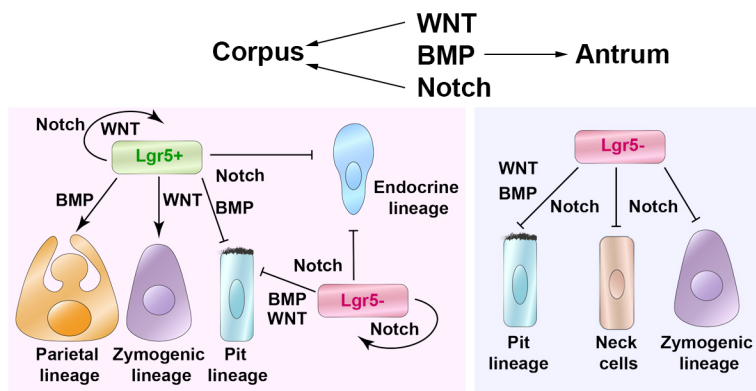
Fig. 7. Working model showing the signalling pathways controlling maintenance and differentiation of the embryonic gastric epithelial progenitors. During mouse embryogenesis, WNT and Notch signals instruct gastric epithelial cells towards corpus identity, whereas BMP signals promote antral fate. Notch then blocks differentiation of the gastric progenitors along all secretory lineages. In the corpus, activation of the WNT pathway leads to the specification of $Lgr5^+$ cells to zymogenic lineage, whereas BMP signals stimulate their differentiation towards parietal lineage. Each of the three pathways inhibits differentiation of the gastric epithelium towards pit cells. In addition to $Lgr5^+$ precursors, $Lgr5^-$ cells have the potential to form entero-endocrine and pit cells.

organoids derived from $Lgr5^+$ progenitors express chief cell markers *Mist1* and *Gif* at levels similar to those found in the adult corpus glands in any tested culture conditions. In contrast, $Lgr5^-$-derived organoids, although activating *Cym*, *Lgr5* and *Axin2* in culture, did not express appreciable levels of chief cell markers. This implies that embryonic $Lgr5^+$ cells are chief cell progenitors. Similar, only $Lgr5^+$-derived organoids express the parietal cell marker *Atp4a*, although at low levels. Our scRNA-seq analysis revealed that a subset of $Lgr5^+$ cells coexpressed *Atp4a*, suggesting that those cells could be parietal cell progenitors.

Both $Lgr5^+$ and $Lgr5^-$ embryonic epithelial cells are plastic at E13.5 and can give rise either to corpus or antrum-like organoids depending on signalling molecules. Whereas WNT and Notch signals are required for the maintenance of the corpus identity, BMP signals are sufficient to promote antrum identity *ex vivo*. The same effects were observed *in vivo*, although less pronounced due to a short treatment of the embryos with the inhibitors. We find that WNT signals are essential for the expression of both *Axin2*- and *Lgr5* both in embryonic stomach and organoids. In contrast, the numbers of $Lgr5^+$ but not of $Axin2^+$ cells increase upon inhibition of either BMP or Notch signalling. Our data suggest that BMP and Notch signals elicit a different cellular response. BMP signalling restricts the number of $Lgr5^+$ cells probably by promoting antrum identity (*Lgr5*-free), whereas Notch signalling inhibits differentiation of the embryonic epithelial progenitors towards secretory neck/chief cells, which express *Lgr5* (Sigal et al., 2019).

The expression of zymogenic chief cell markers strongly depends on the presence of WNT signals. This is not because WNT signals promote corpus identity. Notch signals are also required for the maintenance of the corpus identity but they do not have the same effects on chief cell marker expression. Interestingly, the expression of *Pgc* is negatively regulated by Notch signalling mostly in the antral epithelium. Therefore, we conclude that WNT signalling positively regulates differentiation of embryonic $Lgr5^+$ epithelial cells towards zymogenic cells in the corpus.

Whereas $Lgr5^+$ and Pgc^+ cells are distributed within the whole corpus epithelium, the ectopic $Muc5ac^+$ cells appear only in the ventral epithelium (the lesser curvature) of both corpus and antrum upon inhibition of either the WNT, BMP or Notch pathways. Therefore, either the ventral epithelial cells receive signals promoting differentiation towards $Muc5ac^+$ pit lineage or they express 'ventral-specific' intrinsic factors. scRNA-seq revealed that *Foxq1* and *Klf4* were specifically enriched in $Muc5ac^+$ cells. Consistently, ablation of either *Foxq1* or *Klf4* in the stomach epithelium leads to the loss of MUC5AC$^+$ pit cells in both corpus and antral epithelium (Verzi et al., 2008; Yu et al., 2016). Moreover, enzymes regulating cellular metabolism could act in concert with

transcription factors, including KLF4 (Miao et al., 2020) to regulate gastric progenitor differentiation.

In summary, our study establishes that the embryonic gastric epithelium is molecularly and functionally heterogeneous. Based on the results of organoid assays, we propose that $Lgr5^+$ cells are zymogenic cell progenitors. They depend on WNT, BMP and Notch signals. Our identification of the signals regulating maintenance and differentiation of the gastric progenitors along secretory lineages provides insights into how gastric epithelium is renewed during homeostasis and into possible mechanisms leading to gastric diseases.

MATERIALS AND METHODS
Mouse strains
$Axin2^{Cre-ERT}$, $Lgr5^{EGFP-Cre-ERT}$, $Rosa26^{Cre-ERT2}$, $Rosa26^{tdTomato}$ and $Rosa26^{lacZ}$ mice were obtained from Jackson laboratory. CD1 mice were purchased from Charles Rivers. Mouse colonies were maintained in a certified animal facility as per European guidelines. All experiments were approved by the Landesuntersuchungsamt Rheinland-Pfalz, Germany (G17-5-024 and G18-5-036).

Gastric organoid cultures
Stomachs were dissected from $Lgr5^{EGFP-Cre-ERT}$ mouse embryos at E13.5. One thousand embryonic Lgr5-EGFP$^+$EpCAM$^+$ or EpCAM$^+$ gastric epithelial cells were isolated by FACS directly in 20 μl of gastric medium, mixed with Matrigel (Corning) at a ratio of 1:1 and plated in ibidi chambers (ibidi) with advanced DMEM/F12 medium containing B2-supplement (Gibco), non-essential amino acids, 2 mM L-glutamine, 15 mM HEPES and antibiotics. Both cell culture medium and Matrigel were supplemented with growth factors (Schweiger et al., 2018), including 250 ng/ml human R-spondin1 (Peprotech), 100 ng/ml noggin (R&D systems), 100 ng/ml EGF (R&D systems), 100 ng/ml FGF10 (R&D systems), 3 μM CHIR99021 (Tocris) and 10 μg/ml Y-27632 inhibitor (Tocris). Colony-forming efficiency was calculated by assessing organoid or spheroid formation at 9 days after initiation of cultures. Images were acquired with Leica DM IL microscope at different positions along the z-axis and merged using Adobe Photoshop software.

Intestinal organoid cultures
Intestinal crypts from 4-month-old mice were used to generate intestinal organoids. The proximal mouse small intestines were dissected, cut in pieces of 2 mm^2, placed into 50 ml conical tubes and washed three times for 10 min with 40 ml of PBS containing 5 mM EDTA on a rocking plate at room temperature. Villi were mechanically removed by gentle shaking three times and trituration using a 25 ml pipette. Crypts were separated from the intestine by vigorous shaking twice and passing through a 70 μM filter (BD Falcon). Crypt material was collected by centrifugation at 200×**g** for 3 min, washed twice with PBS and resuspended in the organoids medium (Sato et al., 2009). Crypts were mixed 1:1 with Matrigel (Corning) and plated in ibidi chambers (ibidi) with advanced DMEM/F12 medium containing B27 supplement (Gibco), non-essential amino acids, 2 mM L-glutamine, 15 mM

DEVELOPMENT

HEPES and antibiotics. Both cell culture medium and Matrigel were supplemented with growth factors, including 250 ng/ml human R-spondin1 (Peprotech), 100 ng/ml noggin (R&D systems) and 100 ng/ml EGF (R&D systems). After 9 days in culture, organoids were collected for transcriptome analysis or immunohistochemistry.

Tamoxifen and small molecule administration

Tamoxifen (Sigma-Aldrich) was a 20 mg/ml stock solution in peanut oil (Sigma-Aldrich) and was administered via oral gavage at 0.12 mg/g dam body weight. When P60 stage was required, newborn mice were fed by adoptive lactating CD1 females. Wnt-C59 was administered via oral gavage at 0.01 mg/g dam body weight. LDN193189 was administered via oral gavage at 0.003 mg/g dam body weight. RO4929097 was administered via oral gavage at 0.01 mg/g dam body weight. At indicated time points, stomachs were collected for transcriptome, FACS or histological analysis.

Isolation of gastric epithelial cells using flow cytometry

Stomachs were dissected from $Lgr5^{EGFP-Cre-ERT}$ mouse embryos at E13.5, cut in pieces of 2 mm and incubated for 10 min with 0.15 mg/ml collagenase (Sigma-Aldrich) in PBS at 37°C with shaking at 800 rpm (200 g). Single cell suspensions were collected by centrifugation at 200 g for 4 min, washed twice and resuspended in PBS supplemented with 2% donkey serum. Cells were stained with allophycocyanin (APC)-conjugated anti-EpCAM (1:1000; 17-5791-82; eBioscience) antibody for 15 min at room temperature. Living cells were gated by DAPI dye exclusion. Embryonic gastric epithelial cells were isolated as EpCAM$^+$DAPI$^-$. Embryonic gastric mesenchymal cells were isolated as EpCAM$^-$DAPI$^-$. Embryonic $Lgr5^+$ cells were isolated as EGFP$^+$EpCAM$^+$DAPI$^-$. Fluorescence-activated cell sorting was performed using the BD FACS Aria III SORP cell sorter (85 μm nozzle) and analysed using FlowJo software.

Single-cell RNA-sequencing

To enrich for epithelial cells, single cell suspensions from embryonic stomachs at E13.5 were stained with APC–conjugated anti-EpCAM (1:1000; 17-5791-82; eBioscience) antibody for 15 min at room temperature. Living cells were gated by DAPI dye exclusion. Single cells either EpCAM$^+$ or EpCAM$^-$ were sorted in 96-well plates containing 2.3 μl of lysis buffer (Picelli et al., 2014). FACS was performed using the BD FACS Aria III SORP cell sorter (100 μm nozzle). Spike-in artificial transcripts (ERCC RNA Spike-In Mix, Ambion) from The External RNA Controls Consortium were added in the samples as an internal control. cDNA synthesis and amplification for the individual cells were performed using Smart-Seq2 protocol (Picelli et al., 2014). The cDNA was PCR amplified using Kapa Ready Mix (Kapa Biosystems) for 18 cycles. The quantity and quality of cDNA were assessed with a High Sensitivity DNA Chip (Agilent Technologies). Libraries were generated by Nextera XT DNA Sample Prep Kit (Illumina). In both the tagmentation and final PCR amplification steps, 0.075 ng of cDNA and a quarter of the standard Illumina NexteraXT reaction volume were used. Libraries were sequenced on an Illumina NextSeq500 platform using NextSeq 550 High Output v2 kit (75 cycles).

Single-cell RNA-sequencing data analysis

The data was analysed following the indications of Lun et al. (2016), using the Bioconductor packages scran (McCarthy et al., 2017) and scater (Lun et al., 2016), which implement several tools for quality control and low-level analyses of scRNA-seq data. First, genes not expressed in at least 1% of the cells were removed, and cells not passing a quality threshold were discarded from further analysis. The applied quality threshold takes into account biological and sequencing parameters, defined by the library size, number of genes detected and percentage of mitochondrial RNA, and compares them with the rest of the cells (assuming the distribution of these parameters in the majority of the sampled population displays biologically valid values). Cells with library size or detected genes below two median absolute distances, or showing more than 5% of mitochondrial RNA were discarded (Ilicic et al., 2016; Islam et al., 2011). Gene counts were normalized, removing cell-specific scaling biases and effects between sequenced batches.

Cell subtypes were identified using adaptive branch pruning of hierarchical clustering dendrograms implemented in dynamicTreeCut R package version 1.63-1 (https://CRAN.R-project.org/package=dynamicTreeCut) (Langfelder et al., 2008), using distances between cells defined as correlations using a subset of the 166 most variable and robust genes in the dataset. These genes were identified after decomposing the variance into technical and biological, using a loess model that incorporates the batch and the cell phase as covariates, with biological variance above the 0.99 percentile and detected in multiple cross-cell comparisons.

RNA in situ hybridization

Embryonic stomachs were dissected, fixed overnight in 4% formaldehyde in PBS at 4°C, dehydrated and embedded in paraffin. Sections of 5 μm were rehydrated and treated according to the manufacturer's instructions using RNAscope 2.5 Duplex detection kit (Advanced Cell Diagnostics). Probes for detecting *Atp4a*, *Axin2*, *Bmp4*, *BmpR1a*, *Cym*, *Jag1*, *Lgr5*, *Muc5ac*, *Nkx6-2*, *Notch2*, *Pgc*, *Rspo1*, *Rspo3*, *Tff2*, *Trp63*, *Wnt5a* and *Wnt5b* transcripts were purchased from Advanced Cell Diagnostics. Images were acquired using Leica DM2500 and Olympus IX81 microscopes.

Immunohistochemistry

Embryonic or adult stomachs, as well as gastric organoids were fixed for 20 min in 1% formaldehyde in PBS at room temperature, incubated overnight in 30% sucrose, embedded in OCT and kept at −80°C. Immunohistochemical analyses were performed on 10 μm cryosections. Sections were blocked with 5% donkey serum in 0.1% NP-40 in PBS at room temperature for 1 h. Primary antibodies were incubated overnight at 4°C as follows: 1:1000 anti-EpCAM (APC-conjugated; 17-5791-82; eBiosciences), 1:1000 anti-PDGFRa [562776; phycoerythrin (PE)-conjugated; BD Biosciences], 1:1000 anti-CDH3 (FAB761G; Novus Biologicals), 1:1000 anti-TUBB3 (PRB-435P; Covance), 1:1000 anti-CD45 (561087; PE-conjugated; BD Biosciences), 1:1000 anti-CD31 (553373; PE-conjugated; BD Biosciences), 1:500 anti-MIST1 (NBP2-22478; Novus Biologicals), 1:500 anti-ATP4a (NBP1-88889; Novus Biologicals), 1:500 anti-GIF (NBP1-81610; Novus Biologicals), 1:1000 AlexaFluor594-conjugated-anti-GSII (L21416; Thermo Fisher Scientific), 1:500 anti-MUC5AC (MA5-12178; Thermo Fisher Scientific), 1:300 anti-Ki67 (14-5698-82; Thermo Fisher Scientific), 1:1000 anti-aCASP3 (559565; BD Pharmingen), 1:1000 anti-p63 (GTX102425; Genetex), 1:1000 anti-ISL1 (NBP2-14999; Novus Biologicals) and 1:500 anti-NKX6-3 (NBP1-92185; Novus Biologicals). Diluted (1:300) Alexa Fluor-coupled secondary antibodies (A-11077 and 10424752; Thermo Fisher Scientific) were incubated at room temperature for 1 h. Counterstaining of nuclei was performed with DAPI (1:1000: Sigma-Aldrich). Sections were embedded in Vectashield (Vector Labs).

Periodic acid Schiff staining was performed according to the manufacturer's instructions (Sigma-Aldrich).

To detect $lacZ^+$ cells, stomachs were isolated and fixed with 0.2% glutaraldehyde in PBS for 20 min, washed three times with PBS containing 0.01% NP-40 and 0.01% sodium deoxycholate and incubated for 4 h in the staining solution (5 mM K$_3$[Fe(CN)$_6$], 5 mM K$_4$[Fe(CN)$_6$], 2 mM MgCl$_2$, 0.01% NP-40, 0.01% sodium deoxycholate and 1 mg/ml X-gal in PBS). Images were acquired with Leica TCS SPE, SP8 confocal and Leica M205FA microscopes.

RNA extraction and qRT-PCR

To analyse the expression of glandular markers, only glandular 'transparent' organoids were used. For the analysis of the forestomach markers, only 'dark' keratinized organoids were used. This was done by collecting each type of organoid using a pipette.

Total RNA from gastric or intestinal organoids was isolated using TRI reagent (Sigma-Aldrich). The cells from about ten organoids were resuspended in 300 μl of TRI reagent and incubated for 5 min at room temperature. Chloroform (60 μl) was added followed by vortexing for 15 s. After 10 min incubation at room temperature, samples were centrifuged at 13,000 rpm (16,000 g) for 15 min at 4°C. Following centrifugation, the aqueous phase that retains RNA was transferred into a new tube. Isopropyl alcohol (150 μl) was added and samples incubated for 10 min at room

temperature and centrifuged at 13,000 rpm for 10 min at 4°C. The RNA was washed once in 80% ethanol. The air-dried pellet was resuspended in 20 μl of H$_2$O. Double-stranded cDNA was generated with Superscript III First-Strand Synthesis kit (Thermo Fisher Scientific) according to the manufacturer's instructions. For qRT-PCR, 10 ng of cDNA was used.

For ultralow cell number qRT-PCR analysis, 500 EpCAM$^+$ embryonic gastric cells were isolated by FACS directly in 7 μl of lysis buffer (Clontech) supplemented with 5% RNase inhibitor and stored at −80°C. For each replicate, RNA was isolated from a single embryo. Total mRNA was used for cDNA synthesis using SMARTer v4.0 kit (Clontech) according to the manufacturer's instructions. Amplification was performed for 15 cycles. Expression changes were then normalized to *Tbp*. PCR primers were designed using Primer Blast (http://www.ncbi.nlm.nih.gov/tools/primer-blast/). PCR was performed using SYBR green-containing master mix kit (Applied Biosystems) with ViiA 7 cycler (Applied Biosystems). The mean quantity was calculated from triplicate reactions for each sample.

Statistical analysis

Information on sample size, biological replicas, independent samples, independent experiments and statistical tests used for each experiment are indicated in the figure legends.

Data availability

The single-cell RNA-seq data have been deposited in GEO under accession number GSE137908.

Supplementary information

Supplementary information available online at
https://dev.biologists.org/lookup/doi/10.1242/dev.188839.supplemental

Peer review history

The peer review history is available online at
https://dev.biologists.org/lookup/doi/10.1242/dev.188839.reviewer-comments.pdf

References

Arnold, K., Sarkar, A., Yram, M. A., Polo, J. M., Bronson, R., Sengupta, S., Seandel, M., Geijsen, N. and Hochedlinger, K. (2011). Sox2(+) adult stem and progenitor cells are important for tissue regeneration and survival of mice. *Cell Stem Cell* **9**, 317-329. doi:10.1016/j.stem.2011.09.001

Barker, N., van Es, J. H., Kuipers, J., Kujala, P., van den Born, M., Cozijnsen, M., Haegebarth, A., Korving, J., Begthel, H., Peters, P. J. et al. (2007). Identification of stem cells in small intestine and colon by marker gene Lgr5. *Nature* **449**, 1003-1007. doi:10.1038/nature06196

Barker, N., Huch, M., Kujala, P., van de Wetering, M., Snippert, H. J., van Es, J. H., Sato, T., Stange, D. E., Begthel, H., van den Born, M. et al. (2010). Lgr5(+ve) stem cells drive self-renewal in the stomach and build long-lived gastric units in vitro. *Cell Stem Cell* **6**, 25-36. doi:10.1016/j.stem.2009.11.013

Beumer, J., Artegiani, B., Post, Y., Reimann, F., Gribble, F., Nguyen, T. N., Zeng, H., Van den Born, M., Van Es, J. H. and Clevers, H. (2018). Enteroendocrine cells switch hormone expression along the crypt-to-villus BMP signalling gradient. *Nat. Cell Biol.* **20**, 909-916. doi:10.1038/s41556-018-0143-y

Bockerstett, K. A., Lewis, S. A., Wolf, K. J., Noto, C. N., Jackson, N. M., Ford, E. L., Ahn, T. H. and DiPaolo, R. J. (2020). Single-cell transcriptional analyses of spasmolytic polypeptide-expressing metaplasia arising from acute drug injury and chronic inflammation in the stomach. Version 2. *Gut* **69**, 1027-1038. doi:10.1136/gutjnl-2019-318930

Choi, E., Lantz, T. L., Vlacich, G., Keeley, T. M., Samuelson, L. C., Coffey, R. J., Goldenring, J. R. and Powell, A. E. (2018). Lrig1+ gastric isthmal progenitor cells restore normal gastric lineage cells during damage recovery in adult mouse stomach. *Gut* **67**, 1595-1605. doi:10.1136/gutjnl-2017-313874

Demitrack, E. S., Gifford, G. B., Keeley, T. M., Horita, N., Todisco, A., Turgeon, D. K., Siebel, C. W. and Samuelson, L. C. (2017). NOTCH1 and NOTCH2 regulate epithelial cell proliferation in mouse and human gastric corpus. *Am. J. Physiol. Gastrointest. Liver Physiol.* **312**, G133-G144. doi:10.1152/ajpgi.00325.2016

Han, S., Fink, J., Jörg, D. J., Lee, E., Yum, M. K., Chatzeli, L., Merker, S. R., Josserand, M., Trendafilova, T., Andersson-Rolf, A. et al. (2019). Defining the identity and dynamics of adult gastric isthmus stem cells. *Cell Stem Cell* **25**, 342-356.e7. doi:10.1016/j.stem.2019.07.008

Hayakawa, Y., Ariyama, H., Stancikova, J., Sakitani, K., Asfaha, S., Renz, B. W., Dubeykovskaya, Z. A., Shibata, W., Wang, H., Westphalen, C. B. et al. (2015a). Mist1 expressing gastric stem cells maintain the normal and neoplastic gastric epithelium and are supported by a perivascular stem cell niche. *Cancer Cell* **28**, 800-814. doi:10.1016/j.ccell.2015.10.003

Hayakawa, Y., Jin, G., Wang, H., Chen, X., Westphalen, C. B., Asfaha, S., Renz, B. W., Ariyama, H., Dubeykovskaya, Z. A., Takemoto, Y. et al. (2015b). CCK2R identifies and regulates gastric antral stem cell states and carcinogenesis. *Gut* **64**, 544-553. doi:10.1136/gutjnl-2014-307190

Ilicic, T., Kim, J. K., Kolodziejczyk, A. A., Bagger, F. O., McCarthy, D. J., Marioni, J. C. and Teichmann, S. A. (2016). Classification of low quality cells from single-cell RNA-seq data. *Genome Biol.* **17**, 29. doi:10.1186/s13059-016-0888-1

Islam, S., Kjällquist, U., Moliner, A., Zajac, P., Fan, J.-B., Lönnerberg, P. and Linnarsson, S. (2011). Characterization of the single-cell transcriptional landscape by highly multiplex RNA-seq. *Genome Res.* **21**, 1160-1167. doi:10.1101/gr.110882.110

Kanamori-Katayama, M., Kaiho, A., Ishizu, Y., Okamura-Oho, Y., Hino, O., Abe, M., Kishimoto, T., Sekihara, H., Nakamura, Y., Suzuki, H. et al. (2011). LRRN4 and UPK3B are markers of primary mesothelial cells. *PLoS ONE* **6**, e25391. doi:10.1371/journal.pone.0025391

Kim, T.-H. and Shivdasani, R. A. (2011). Notch signaling in stomach epithelial stem cell homeostasis. *J. Exp. Med.* **208**, 677-688. doi:10.1084/jem.20101737

Kretzschmar, K. and Clevers, H. (2017). Wnt/β-catenin signaling in adult mammalian epithelial stem cells. *Dev. Biol.* **428**, 273-282. doi:10.1016/j.ydbio.2017.05.015

Langfelder, P., Zhang, B. and Horvath, S. (2008). Defining clusters from a hierarchical cluster tree: the Dynamic Tree Cut package for R. *Bioinformatics* **24**, 719-720. doi:10.1093/bioinformatics/btm563

Leushacke, M., Tan, S. H., Wong, A., Swathi, Y., Hajamohideen, A., Tan, L. T., Goh, J., Wong, E., Denil, S. L. I. J., Murakami, K. et al. (2017). Lgr5-expressing chief cells drive epithelial regeneration and cancer in the oxyntic stomach. *Nat. Cell Biol.* **19**, 774-786. doi:10.1038/ncb3541

Lun, A. T. L., McCarthy, D. J. and Marioni, J. C. (2016). A step-by-step workflow for low-level analysis of single-cell RNA-seq data. *F1000Research* **5**, 2122. doi:10.12688/f1000research.9501.1

Lustig, B., Jerchow, B., Sachs, M., Weiler, S., Pietsch, T., Karsten, U., van de Wetering, M., Clevers, H., Schlag, P. M., Birchmeier, W. et al. (2002). Negative feedback loop of Wnt signaling through upregulation of conductin/axin2 in colorectal and liver tumors. *Mol. Cell. Biol.* **22**, 1184-1193. doi:10.1128/MCB.22.4.1184-1193.2002

Maloum, F., Allaire, J. M., Gagné-Sansfaçon, J., Roy, E., Belleville, K., Sarret, P., Morisset, J., Carrier, J. C., Mishina, Y., Kaestner, K. H. et al. (2011). Epithelial BMP signaling is required for proper specification of epithelial cell lineages and gastric endocrine cells. *Am. J. Physiol. Gastrointest. Liver Physiol.* **300**, G1065-G1079. doi:10.1152/ajpgi.00176.2010

Matsuo, J., Kimura, S., Yamamura, A., Koh, C. P., Hossain, M. Z., Heng, D. L., Kohu, K., Voon, D. C.-C., Hiai, H., Unno, M. et al. (2017). Identification of stem cells in the epithelium of the stomach corpus and antrum of mice. *Gastroenterology* **152**, 218-231.e14. doi:10.1053/j.gastro.2016.09.018

McCarthy, D. J., Campbell, K. R., Lun, A. T. L. and Willis, Q. F. (2017). Scater: pre-processing, quality control, normalisation and visualisation of single-cell RNA-seq data in R. *Bioinformatics* **33**, 1179-1186. doi:10.1093/bioinformatics/btw777

McCracken, K. W., Aihara, E., Martin, B., Crawford, C. M., Broda, T., Treguier, J., Zhang, X., Shannon, J. M., Montrose, M. H. and Wells, J. M. (2017). Wnt/β-catenin promotes gastric fundus specification in mice and humans. *Nature* **541**, 182-187. doi:10.1038/nature21021

Miao, Z.-F., Adkins-Threats, M., Burclaff, J. R., Osaki, L. H., Sun, J.-X., Kefalov, Y., He, Z., Wang, Z.-N. and Mills, J. C. (2020). A metformin-responsive metabolic pathway controls distinct steps in gastric progenitor fate decisions and maturation. *Cell Stem Cell* **26**, 910-925.e6. doi:10.1016/j.stem.2020.03.006

DEVELOPMENT

Nigmatullina, L., Norkin, M., Dzama, M. M., Messner, B., Sayols, S. and Soshnikova, N. (2017). Id2 controls specification of Lgr5+ intestinal stem cell progenitors during gut development. *EMBO J.* **36**, 869-885. doi:10.15252/embj. 201694959

Picelli, S., Faridani, O. R., Björklund, A. K., Winberg, G., Sagasser, S. and Sandberg, R. (2014). Full-length RNA-seq from single cells using Smart-seq2. *Nat. Protoc.* **9**, 171-181. doi:10.1038/nprot.2014.006

Sato, T., Vries, R. G., Snippert, H. J., van de Wetering, M., Barker, N., Stange, D. E., van Es, J. H., Abo, A., Kujala, P., Peters, P. J. et al. (2009). Single Lgr5 stem cells build crypt-villus structures in vitro without a mesenchymal niche. *Nature* **459**, 262-265. doi:10.1038/nature07935

Schweiger, P. J., Clement, D. L., Page, M. E., Schepeler, T., Zou, X., Sirokmány, G., Watt, F. M. and Jensen, K. B. (2018). Lrig1 marks a population of gastric epithelial cells capable of long-term tissue maintenance and growth in vitro. *Sci. Rep.* **8**, 15255. doi:10.1038/s41598-018-33578-6

Sigal, M., Logan, C. Y., Kapalczynska, M., Mollenkopf, H.-J., Berger, H., Wiedenmann, B., Nusse, R., Amieva, M. R. and Meyer, T. F. (2017). Stromal R-spondin orchestrates gastric epithelial stem cells and gland homeostasis. *Nature* **548**, 451-455. doi:10.1038/nature23642

Sigal, M., Reinés, M. D. M., Müllerke, S., Fischer, C., Kapalczynska, M., Berger, H., Bakker, E. R. M., Mollenkopf, H.-J., Rothenberg, M. E., Wiedenmann, B. et al. (2019). R-spondin-3 induces secretory, antimicrobial Lgr5+ cells in the stomach. *Nat. Cell Biol.* **21**, 812-823. doi:10.1038/s41556-019-0339-9

Spencer-Dene, B., Sala, F. G., Bellusci, S., Gschmeissner, S., Stamp, G. and Dickson, C. (2006). Stomach development is dependent on fibroblast growth factor 10/fibroblast growth factor receptor 2b-mediated signaling. *Gastroenterology* **130**, 1233-1244. doi:10.1053/j.gastro.2006.02.018

Stange, D. E., Koo, B.-K., Huch, M., Sibbel, G., Basak, O., Lyubimova, A., Kujala, P., Bartfeld, S., Koster, J., Geahlen, J. H. et al. (2013). Differentiated Troy+ chief cells act as reserve stem cells to generate all lineages of the stomach epithelium. *Cell* **155**, 357-368. doi:10.1016/j.cell.2013.09.008

Tanaka, K., Kitagawa, Y. and Kadowaki, T. (2002). Drosophila segment polarity gene product porcupine stimulates the posttranslational N-glycosylation of wingless in the endoplasmic reticulum. *J. Biol. Chem.* **277**, 12816-12823. doi:10.1074/jbc.M200187200

Verzi, M. P., Khan, A. H., Ito, S. and Shivdasani, R. A. (2008). Transcription factor foxq1 controls mucin gene expression and granule content in mouse stomach surface mucous cells. *Gastroenterology* **135**, 591-600. doi:10.1053/j.gastro.2008. 04.019

Willet, S. G. and Mills, J. C. (2016). Stomach organ and cell lineage differentiation: from embryogenesis to adult homeostasis. *Cell Mol. Gastroenterol. Hepatol.* **2**, 546-559. doi:10.1016/j.jcmgh.2016.05.006

Yoshioka, T., Fukuda, A., Araki, O., Ogawa, S., Hanyu, Y., Matsumoto, Y., Yamaga, Y., Nakanishi, Y., Kawada, K., Sakai, Y. et al. (2019). Bmi1 marks gastric stem cells located in the isthmus in mice. *J. Pathol.* **248**, 179-190. doi:10. 1002/path.5244

Yu, T., Chen, X., Lin, T., Liu, J., Li, M., Zhang, W., Xu, X., Zhao, W., Liu, M., Napier, D. L. et al. (2016). KLF4 deletion alters gastric cell lineage and induces MUC2 expression. *Cell Death Dis.* **7**, e2255. doi:10.1038/cddis.2016.158

DEVELOPMENT